Solid NMR Techniques for Glass and Glass-Ceramics Studies

Thibault Charpentier

CEA / IRAMIS / SIS2M - CEA Saclay

NUCLEATION ET CRISTALLISATION DES MATERIAUX VITREUX
GDR Verre, 13-17 mai 2013

The Zeeman Interaction and Larmor Frequency

The NMR spectrum of an isolated nucleus . . .

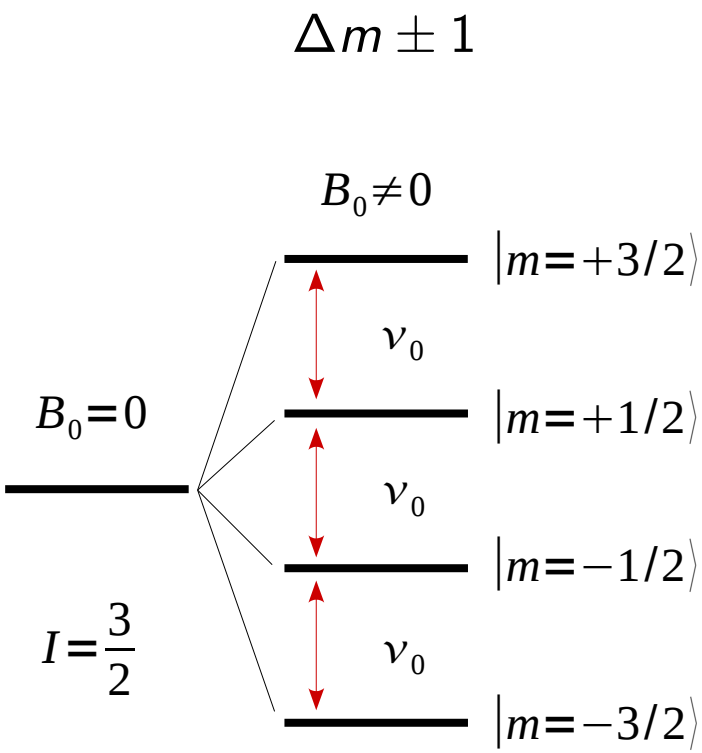

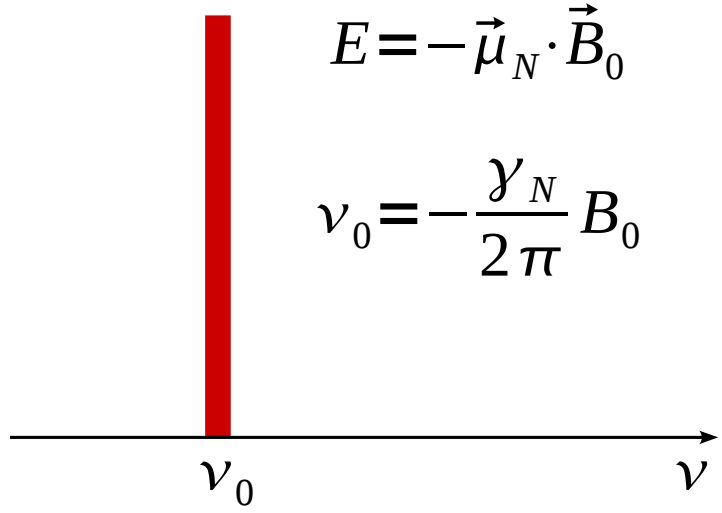

The Larmor frequency and its NMR spectrum.

The Zeeman effect

No information on the chemical surrounding

$$(\hbar)\, H = -\hbar\gamma_N \vec{I} \cdot \vec{B}_0$$

NMR and the Periodic Table

One-half and *quadrupolar nuclei*

- Isotope, Nuclear Spin
- Natural Abundance
- Gyromagnetic ratio γ (rad/s/T)
  $\omega_0 = 2\pi\nu_0 = -\gamma B_0$
- Quadrupolar Moment Q (see Pyykkö)

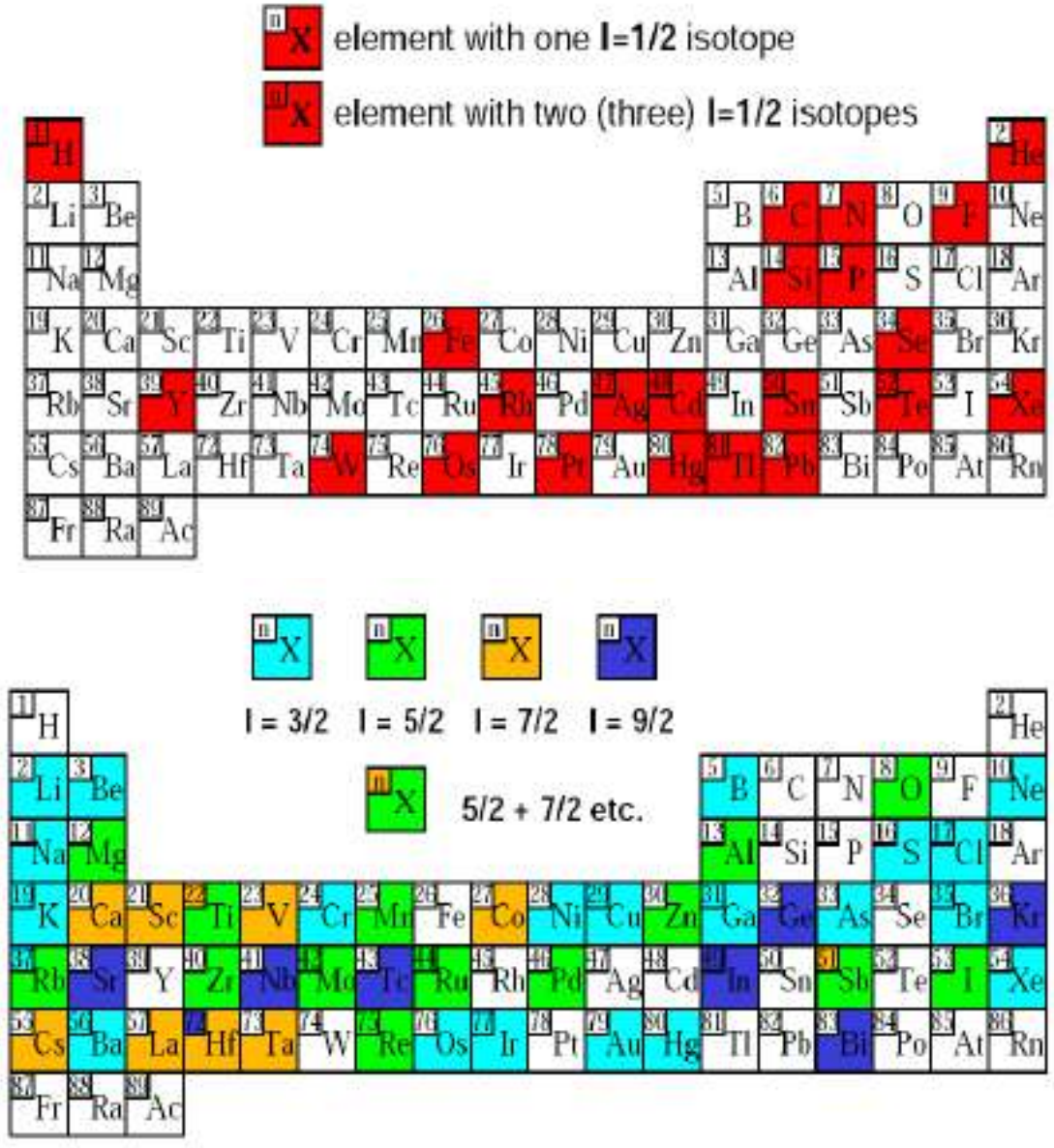

Nuclear waste Glasses: R7T7 & SON68

A complex borosilicate glass comprising more than 30 oxides

oxide	% (w)
$^{29}SiO_2$	45.12
$^{27}Al_2O_3$	4.87
$^{11}B_2O_3$	13.92
$^{6,7}Li_2O$	1.97
$^{23}Na_2O$	9.78
^{43}CaO	4.01
ZrO_2	0.99
ZnO	2.48
Fe_2O_3	2.89
P_2O_5	0.28
NiO	0.41
Cr_2O_3	0.50
Fission Products	10.35
Actinides	0.89
Platinoides	1.54

For Solid State NMR studies:
Simplified Compositions
3-8 oxides
(many) NMR Probes

^{11}B ^{27}Al ^{29}Si ^{23}Na $^{6,7}Li$ ^{17}O ^{43}Ca

^{17}O, 0.037% Nat. Abundance
Isotopic enrichment required

NMR sensitivity

Equilibrium Nuclear Magnetization

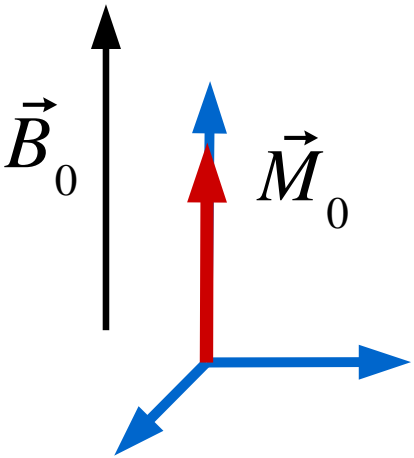

Larmor Precession at ν_0

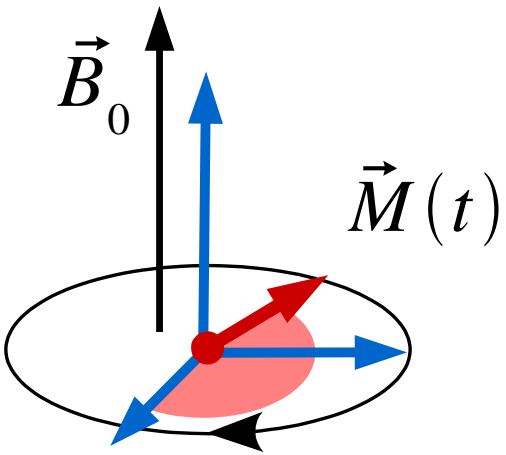

M_0: Nuclear Magnetization at Equilibrium is given by the Curie Law

$$\vec{M}_0 = \sum_i \vec{\mu}_i = \chi_0 \vec{B}_0 \propto \exp\{-\Delta E/kT\}$$

$$\chi_0 = N_I \frac{\gamma_I^2 \hbar^2 I(I+1)}{3kT} B_0$$

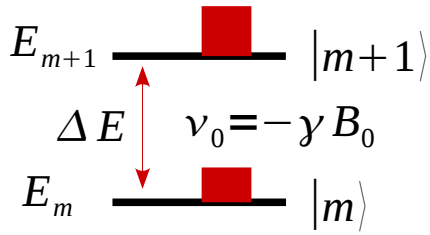

- Small polarization 10^{-3} to 10^{-6}
- Signal $\propto N_I$ Quantitativity
- Signal $\propto B_0$ High Field
- signal $\propto \gamma_I^2$

Pulsed NMR

The Basic NMR Experiment . . . One pulse !

M_0: Nuclear Magnetization at Equilibrium

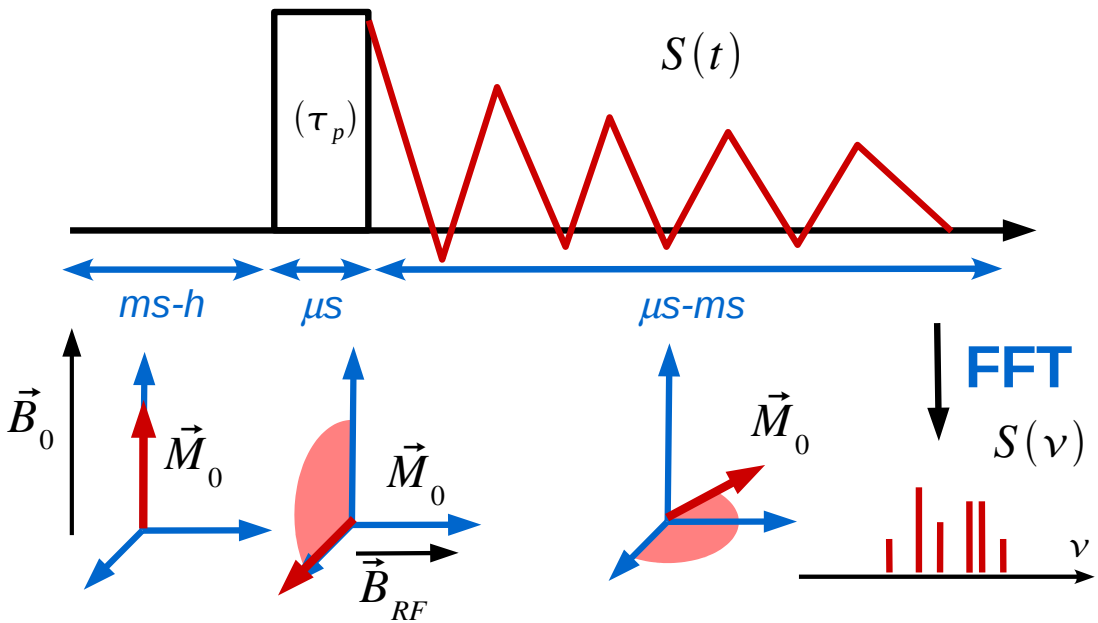

$$\begin{aligned} \vec{M}(0) &= M_0\vec{z} \\ \vec{M}(\tau_p) &= M_0\vec{x} \\ S(t) &= M_0 e^{-i\nu_0 t} e^{-\frac{t}{T_2}} \end{aligned}$$

$$S(\nu) = \int_0^\infty dt\, S(t) e^{-i2\pi\nu t} \approx \sum_{k=0}^{N-1} S(t_k) e^{-i2\pi\nu t_k} = L(\nu - \nu_0)$$

Lineshape $L(\nu)$: Gaussian, Lorentzian . . .

Pulsed NMR in powder solids

The Basic NMR Experiment: Fourier Transform

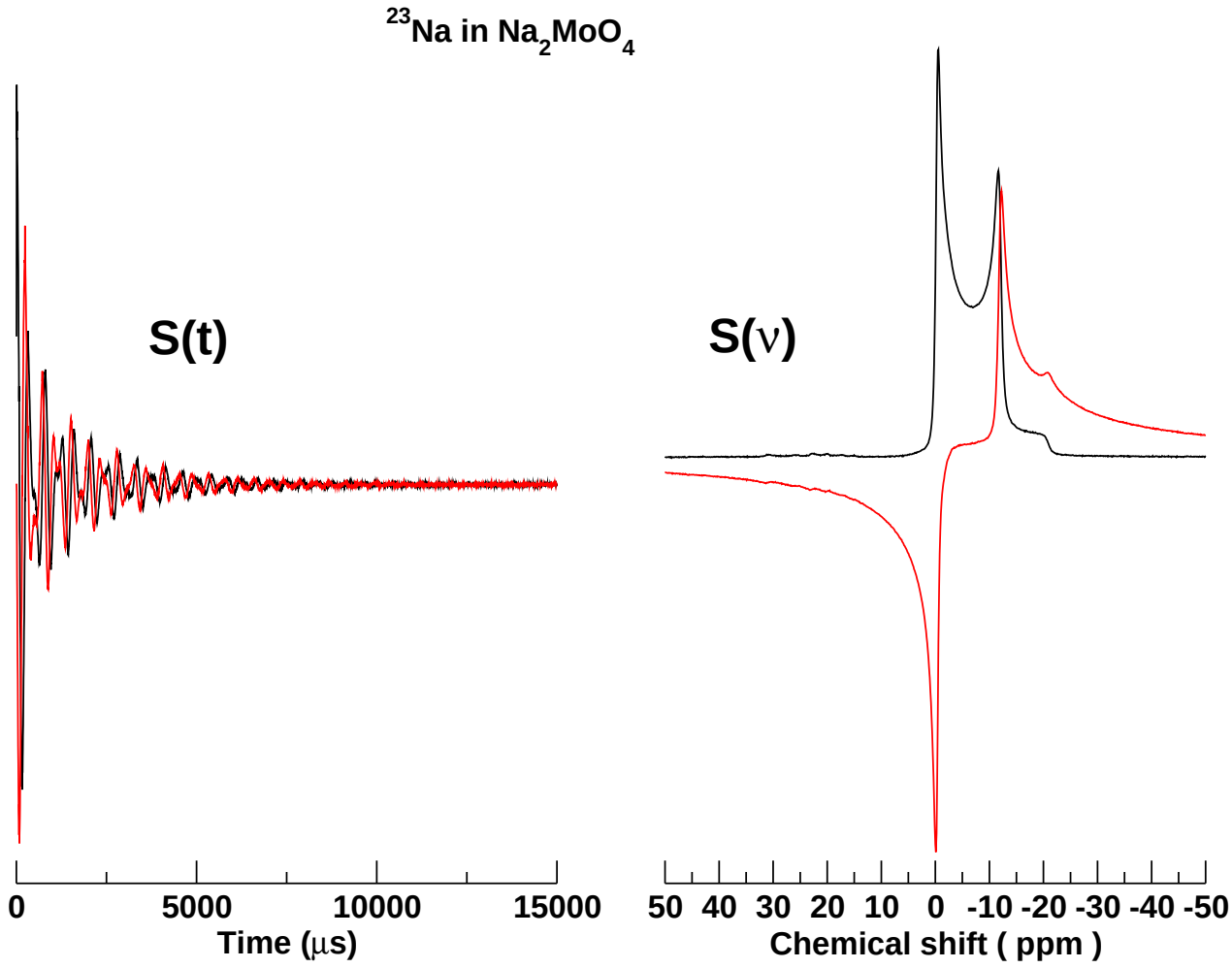

NMR Interactions for NMR spectroscopists

Effects of the *local* magnetic fields . . .

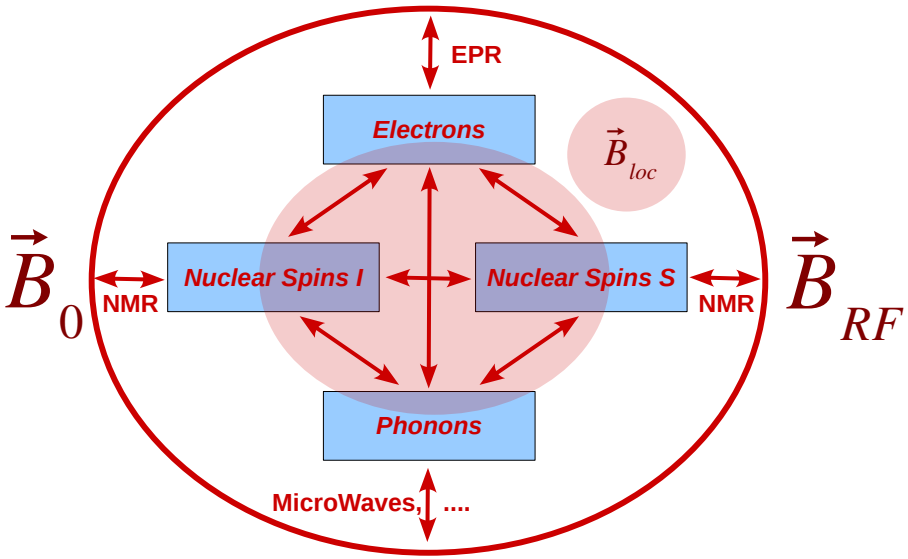

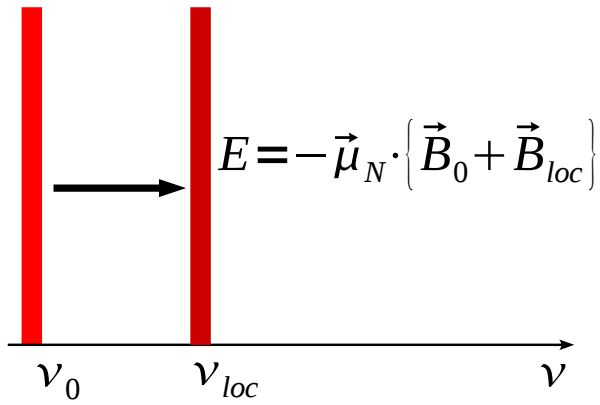

The NMR spectrum

Information on the chemical surrounding

$$(\hbar)\, H = -\hbar\gamma_N \vec{I} \cdot \left\{ \vec{B}_0 + \vec{B}_{loc} \right\} = H_Z + H_{\text{inter.}}$$

$$(\hbar)\, H = H_Z + H_{CS} + H_Q + H_J + H_D + \ldots$$

CS: Chemical Shift, Q: Quadrupolar, J: J couplings, D: Dipolar

NMR interactions (without equations . . .)

One-Spin Interactions
Magnetic Shielding /
Chemical shift

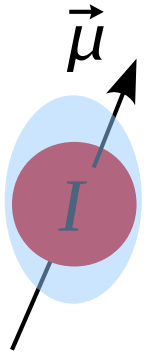

Electif Field Gradient (EFG)

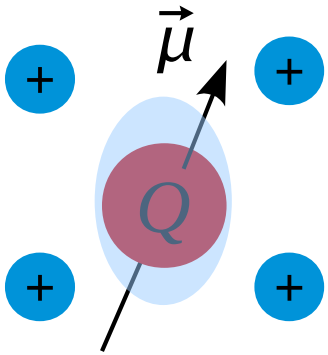

Two-Spins Interactions
Dipolar: through Space

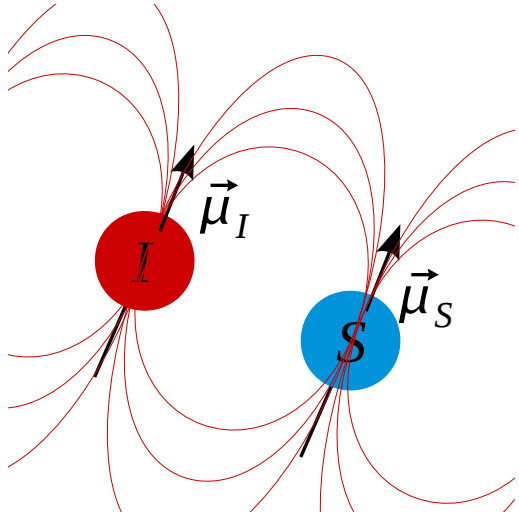

J: through bond

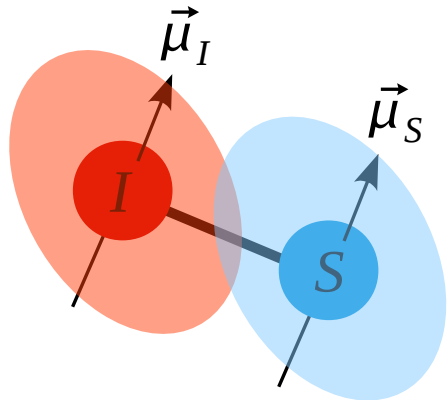

NMR interactions: The *effective* Hamiltonian

$$\mathcal{H}_S(\text{NMR}) = \underbrace{-\hbar \sum_i \gamma_i \vec{I}_i \left(\mathbf{1} - \boldsymbol{\sigma}\right) \vec{B}_0 + \sum_{i,|I_i|\geq 1} \vec{I}_i \mathbf{Q}_{ii} \vec{I}_i}_{One-spin:\ chemical\ environment} + \underbrace{\frac{\hbar^2}{2} \sum_i \sum_{j\neq i} \gamma_i \gamma_j \vec{I}_i \left(\mathbf{D}_{ij} + \mathbf{J}_{ij}\right) \vec{I}_j}_{Two-spins:\ spatial\ and\ through\ bond\ proximities}$$

$\vec{B}_0$	External magnetic field / Internal Interactions
$\vec{I}_i$	Nuclear spin operators $\vec{\mu}_i = \gamma_i \hbar \vec{I}_i$ (NMR)
$\boldsymbol{\sigma}$	Nuclear magnetic shielding tensor (chemical shift) (DFT)
$\mathbf{Q}_{ii}$	Nuclear quadrupolar coupling tensor ($\lvert I_i \rvert \geq 1$) (DFT)
$\mathbf{D}_{ij}$	Nuclear magnetic dipolar coupling tensor (structure)
$\mathbf{J}_{ij}$	Indirect nuclear spin-spin coupling tensor (DFT)

Multiple interactions: complex spectrum. High Resolution $\Rightarrow \boldsymbol{\sigma}_{iso}$

NMR Interactions are Anisotropic . . .

. . . NMR spectra of a single molecule (crystal)

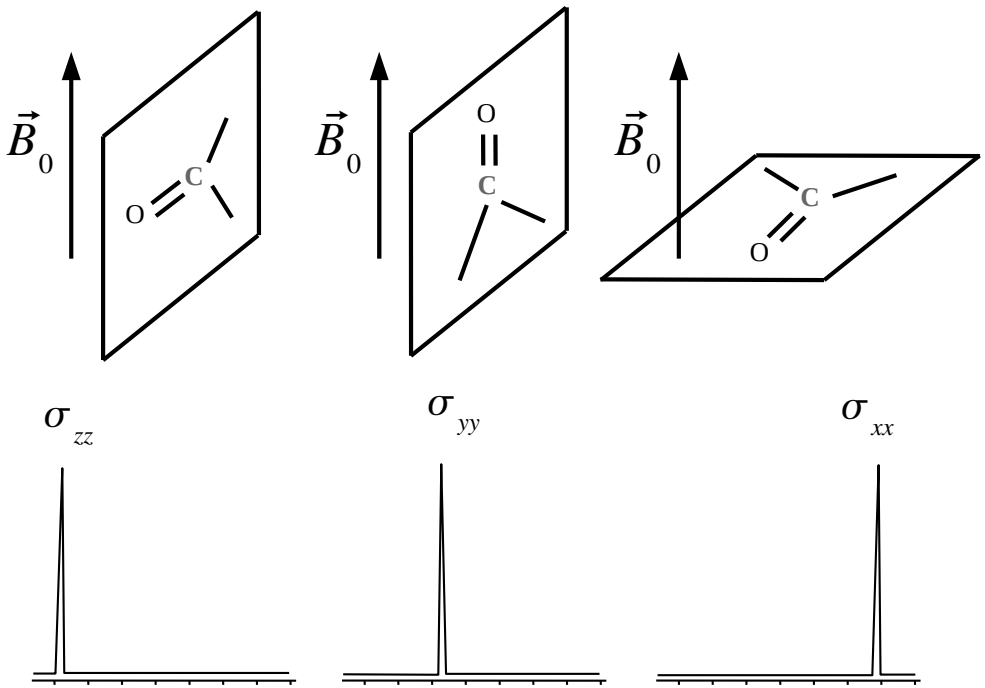

The NMR frequency depends on the orientation with respect to $\vec{B}_0$

$$\nu - \nu_0 = \nu_{int}(\Omega)$$

Single crystal NMR exists . . . but amorphous materials ?

NMR Interactions are Anisotropic . . .

. . . NMR spectrum (CSA) of a powder

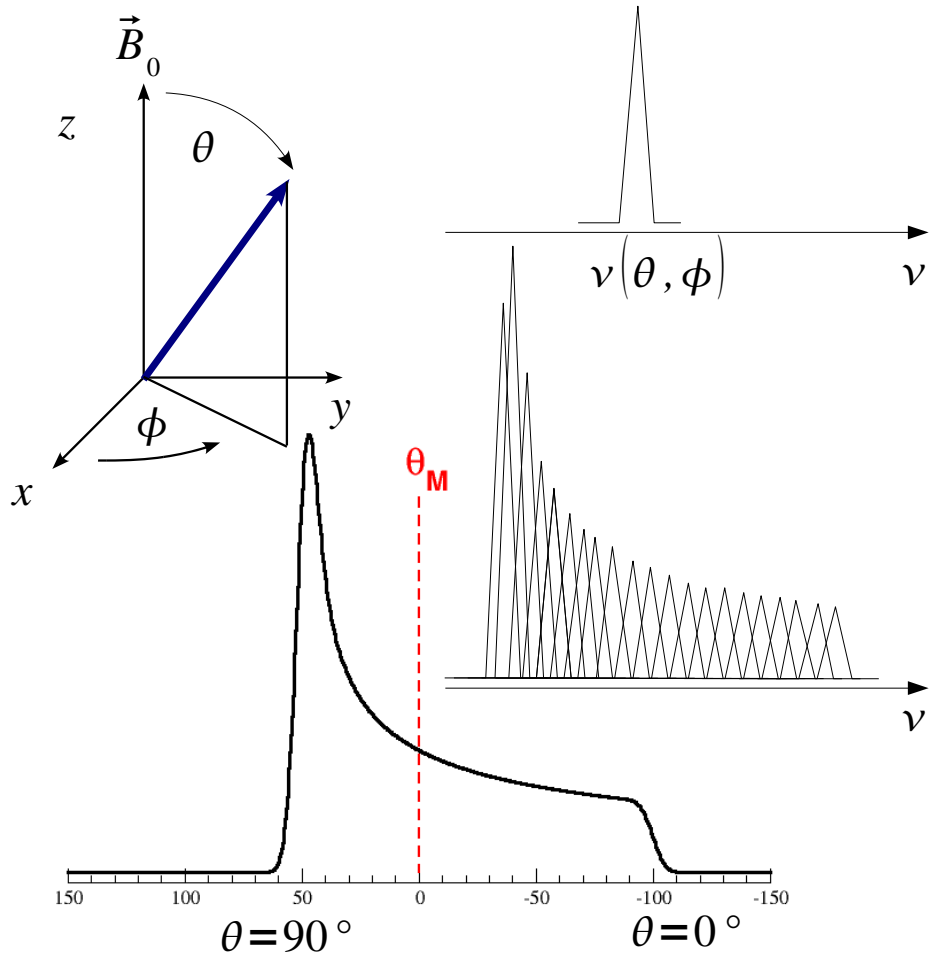

The powder average

$$S(t) = \int \sin\theta d\theta d\phi \times \exp\{-i\nu(\theta,\phi)t\}$$

$\Rightarrow$ A glass sample provides a powder spectrum.

NMR Interactions are Anisotropic . . .

. . . but in liquids only the isotropic part is effective

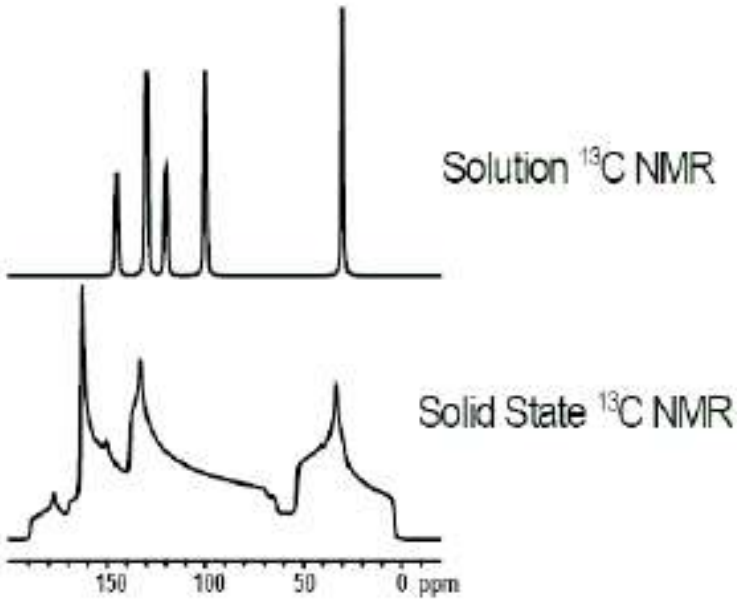

Motional averaging

- Motions affect the anisotropic lineshape.
- In the case of fast motional averaging (vs Larmor frequency), a narrow line at the isotropic frequency.
- Brownian Motion in liquid
- Motions (fluctuations) induce Relaxation

$$\overline{H\left(\Omega(t)\right) = H_{iso} + H_{ani}\left(\Omega(t)\right)} \text{ with}$$
$$\overline{H_{ani}\left(\Omega(t)\right)} = 0 \text{ at the Larmor time scale } (\ 1/\nu_0)$$

The Zeeman Truncation in High Field NMR

Only the part along B_0 is *NMR active* to first order.

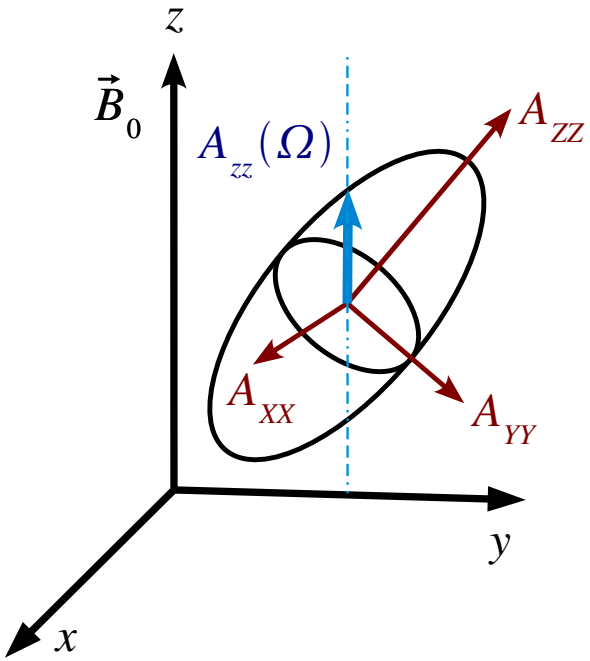

In case of 1-spin interaction, only A_{zz} (in the reference frame) contributes to first order to the NMR frequency.

Because $B_0 \gg B_{loc}$ (or $H_Z \gg H_{int}$), we have the *secular* approximation

$$H_{int} \approx H_{CS}^{(1)} + H_Q^{(1)} + H_Q^{(2)} + H_J^{(1)} + H_D^{(1)} \ldots$$

Typical strength of NMR interactions

- Z: 10-1000 MHz
- CS: kHz
- Q: MHz (up to second order)
- D: kHz
- J: Hz

The shielding / Chemical Shift Tensor

NMR static powder lineshape

$$H_{CS} = \gamma \vec{I} \boldsymbol{\sigma} \vec{B}_0 \approx \gamma B_0 \sigma_{zz}(\Omega) I_z \Rightarrow \nu_{NMR}^{CS} = \delta_{iso} + \delta_{CS} R_{20}(\Omega, \eta)$$

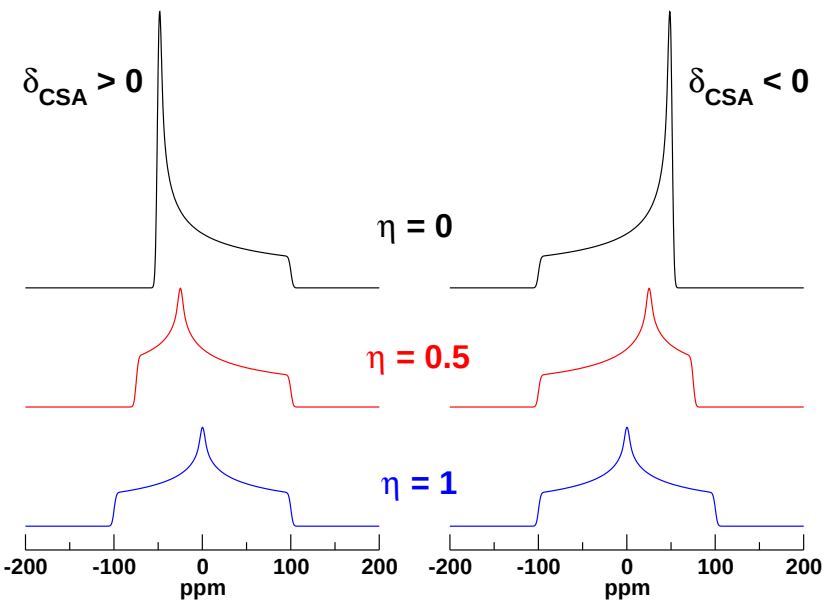

- δ_{iso} : isotropic chemical shift (position)
- δ_{cs}: chemical shift anisotropy (width)
- η: assymetry (shape)

NMR measures the *chemical shift* tensor $\boldsymbol{\delta}$ (ppm):

$$\delta_{iso}^{exp}(\text{ppm}) = 10^6 \left(\frac{\nu - \nu_{ref}}{\nu_{ref}} \right)$$

The NMR frequency of the *central transition* can be written as

$$\nu_{-1/2,+1/2}(\Omega) - \nu_0 = \delta_{iso} + \delta_{CS} R_{20}(\Omega, \eta)$$

The Chemical Shift Anisotropy

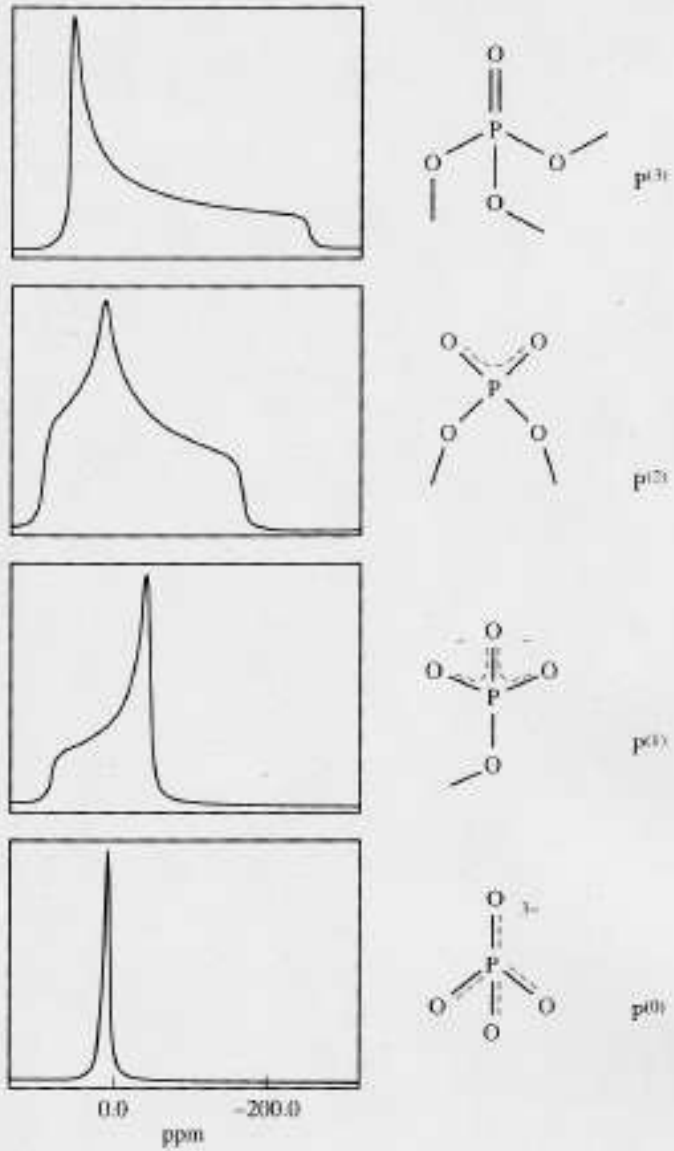

Figure 26 Phosphorus sites in alkali phosphate glasses and their wideline ^{31}P NMR anisotropic chemical shift powder patterns. The terminology used here is analogous to that defined in Figure 7(a) (Reproduced by permission of Pergamon Press from H. Eckert, *Prog. Nucl. Magn. Reson.*, 1992, **24**, 159)

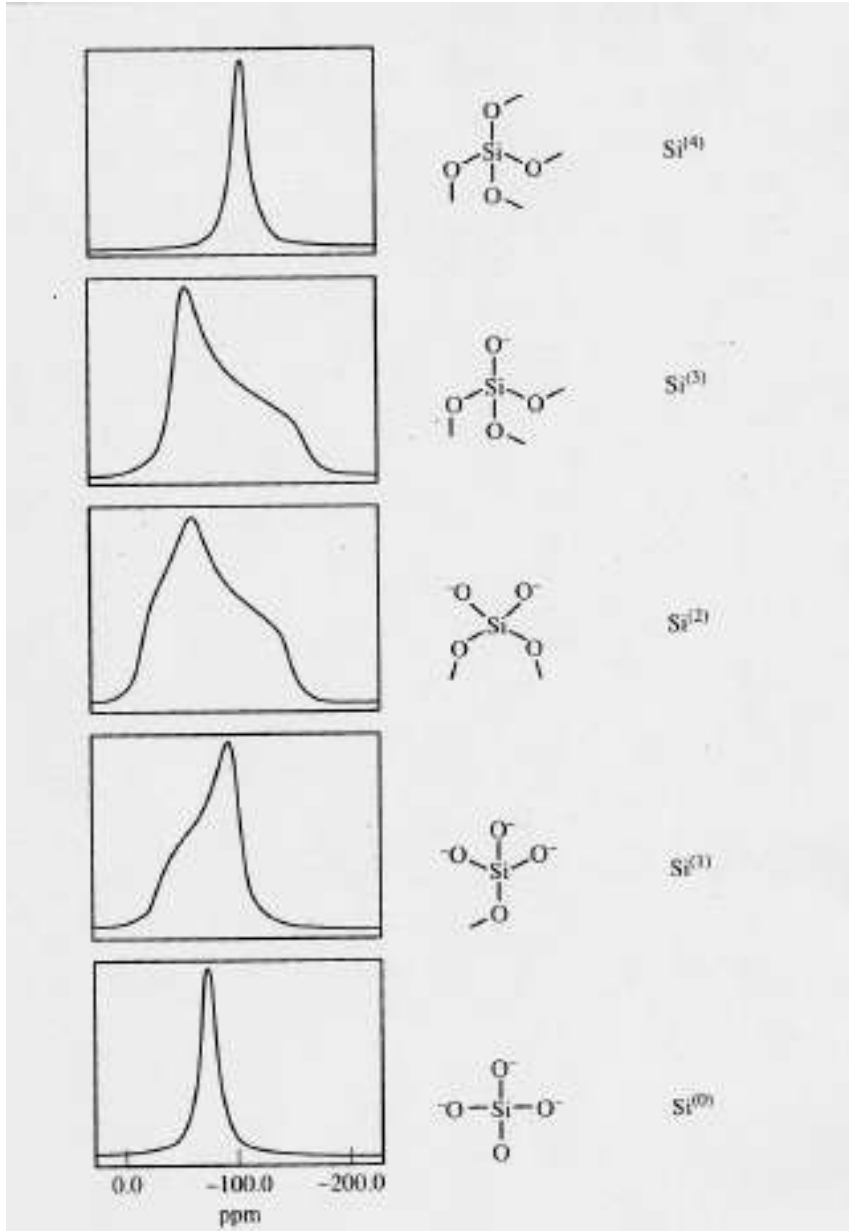

Figure 7 $Si^{(n)}$ (also labeled $Q^{(n)}$ in the literature) species in alkali silicate glasses and their ^{29}Si chemical shift powder patterns (Reproduced by permission of Pergamon Press from H. Eckert, *Prog. Nucl. Magn. Reson.*, 1992, **24**, 159)

The quadrupolar interaction

from electric field gradient. Only for $I \geq 1$.

Because of its large strength (kHz-MHz), quadrupolar Hamiltonian are often accounted for up to second order (^{23}Na,^{17}O,^{27}Al,^{11}B...) depending on the local environment of the nucleus.

The electric field gradient $\mathbf{V}$ is a symmetric traceless ($V_{XX} + V_{YY} + V_{ZZ} = 0$) tensor.

$$C_Q = \frac{eQ}{h} V_{ZZ} \, , \eta_Q = \frac{V_{XX} - V_{YY}}{V_{ZZ}} \, , V_{iso} = 0$$

C_Q: quadrupolar couping constant, η_Q: quadrupolar asymmetry parameter.

The quadrupolar interaction

NMR static powder lineshape

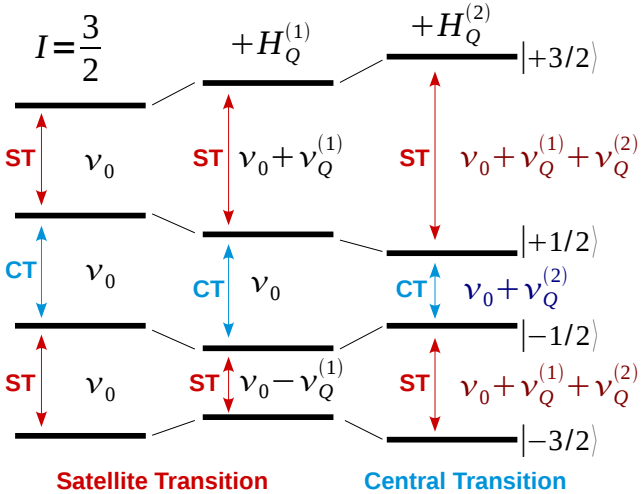

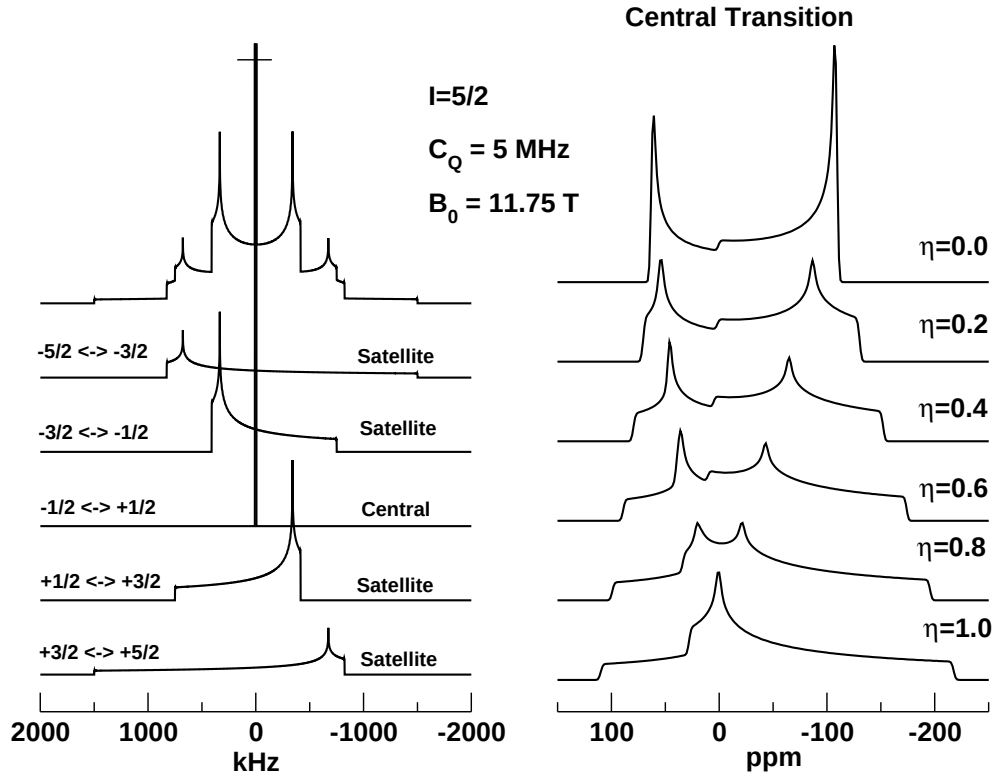

CT transition afftected only to second order: $\Rightarrow$ narrow line

The NMR frequency of the *central transition* can be written as

$$\nu_{-1/2,+1/2}(\Omega) - \nu_0 = a_0^{(2)} + a_2^{(2)} R_{20}(\Omega,\eta) + a_4^{(4)} R_{40}(\Omega,\eta)$$

High Resolution NMR

Why Magic Angle Sample Spinning ?

$R_{20}(\Omega) \propto 3\cos^2\theta - 1$

Method: Reduce all orientation to an *effective magic angle* orientation !

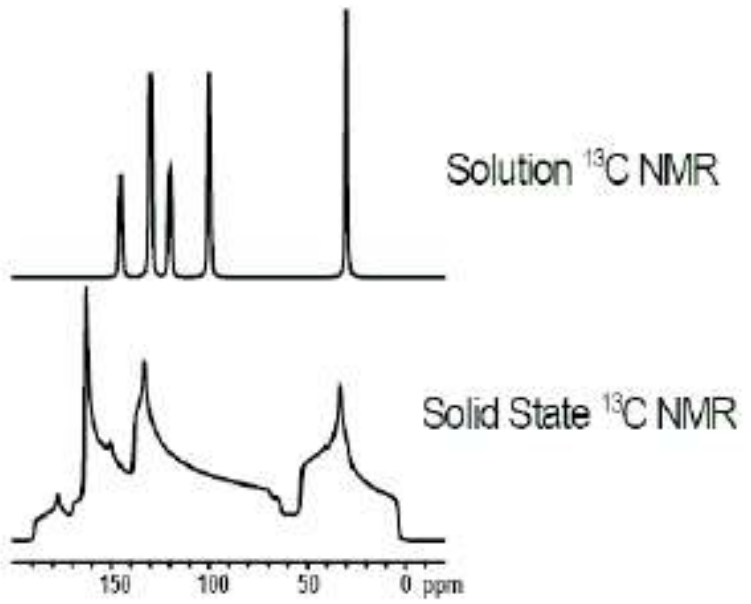

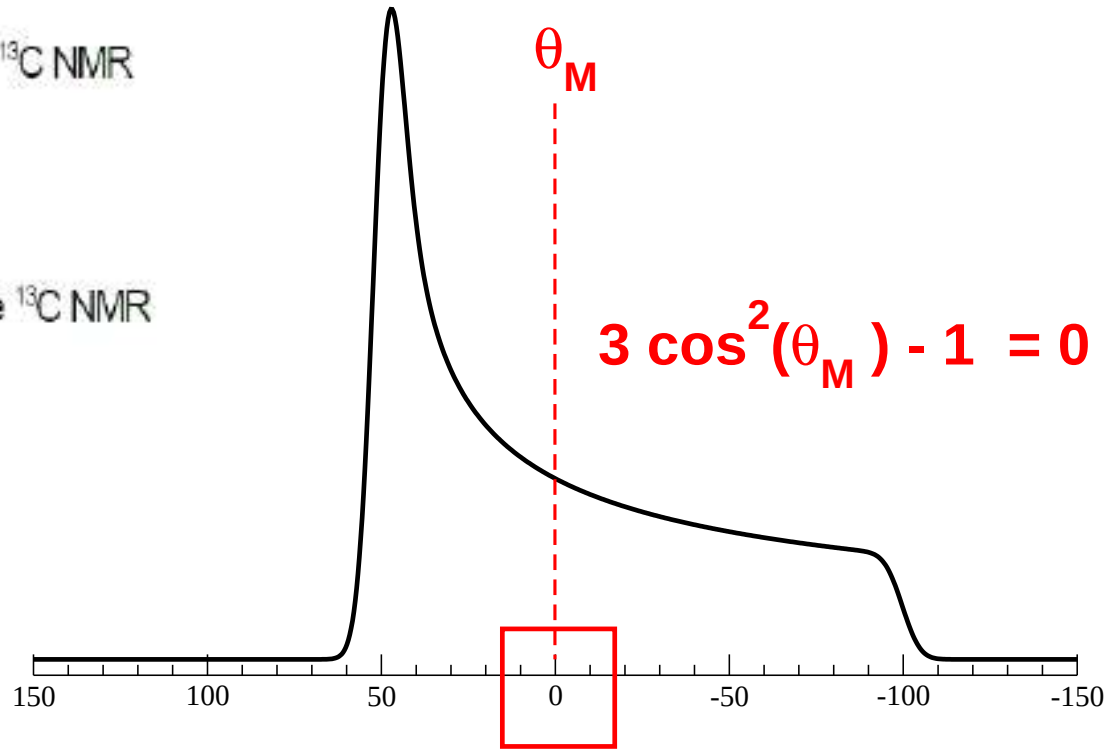

High Resolution NMR

Magic Angle Sample Spinning: a *coherent* averaging approach

$$\mathbf{A}\left(\Omega(t)\right) = A_{iso}\mathbf{1} + \overline{\mathbf{A}}(\theta_M) + \widetilde{\mathbf{A}}(t)$$

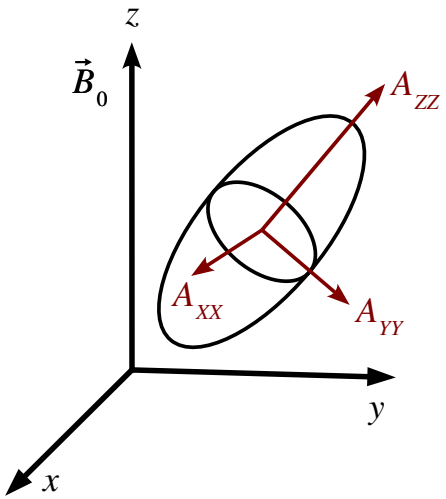

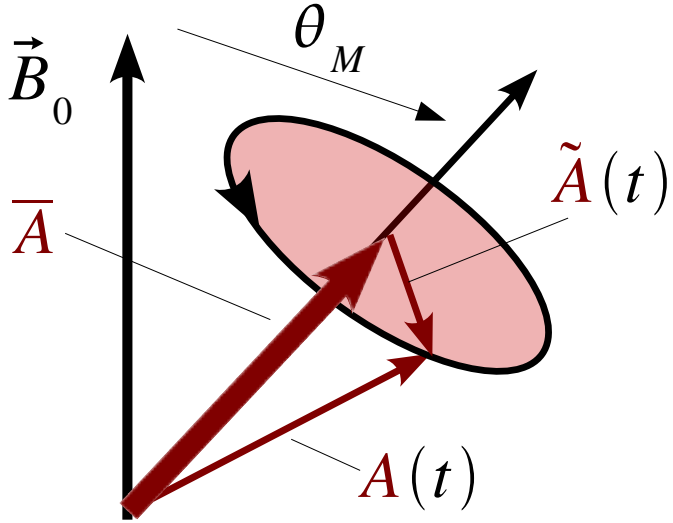

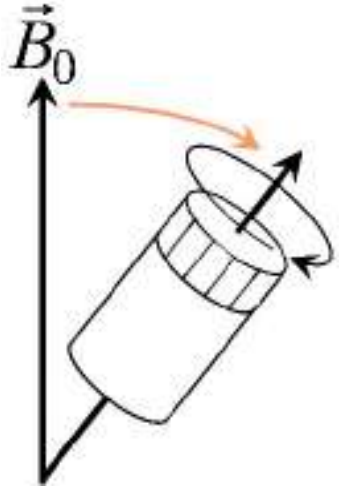

Magic Angle: $\overline{A}(\theta_M) = \overline{A} = 0$ (Fast) Spinning $\overline{\widetilde{A}(t)} = 0$

Effective **A** reduces (to first order) to $A_{iso}\mathbf{1}$.

Magic Angle Sample Spinning: Principles

Introducing a *coherent* sample motion

Static Sample

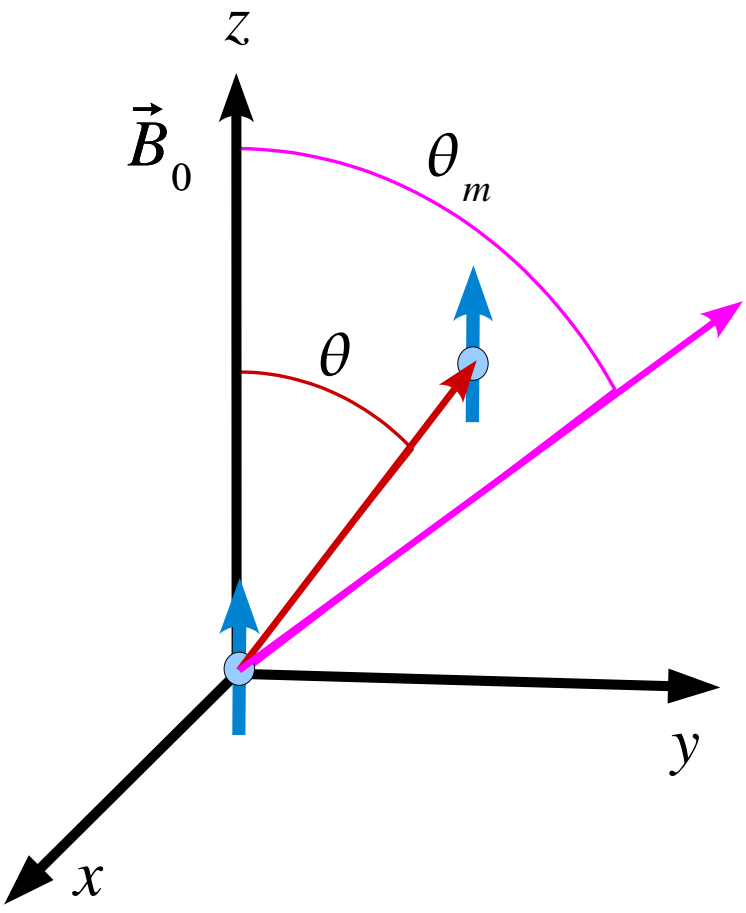

Interaction along θ

Spinning the Sample around the Magic Angle θ_m

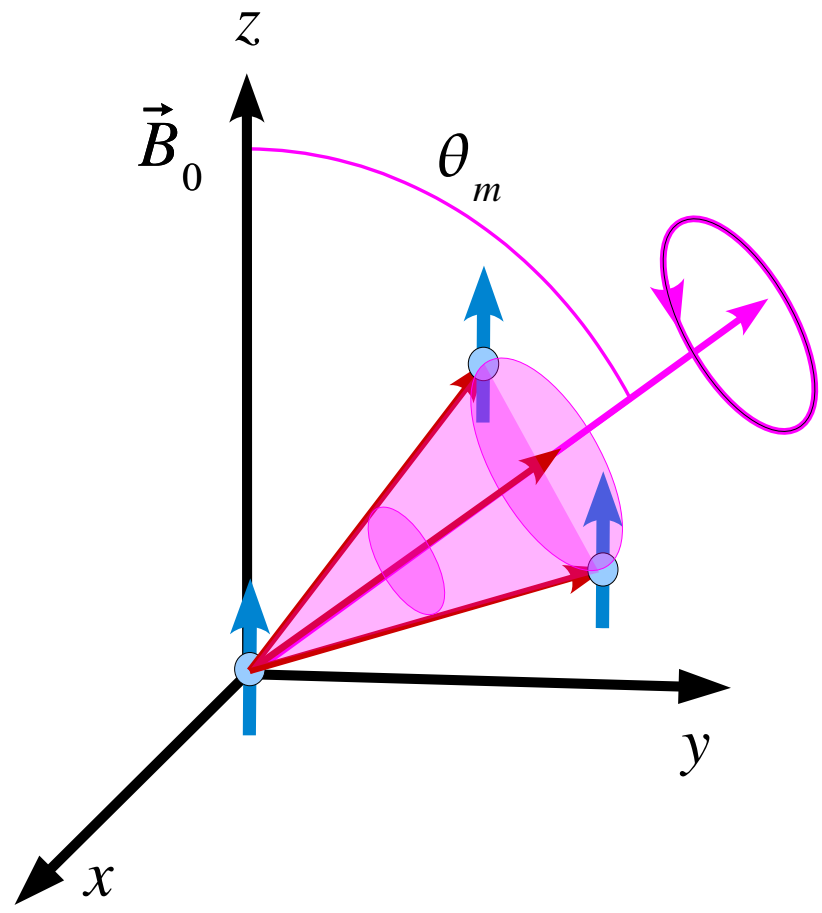

Effective interaction along θ_m

High Resolution NMR

Magic Angle (Sample) Spinning for I=1/2

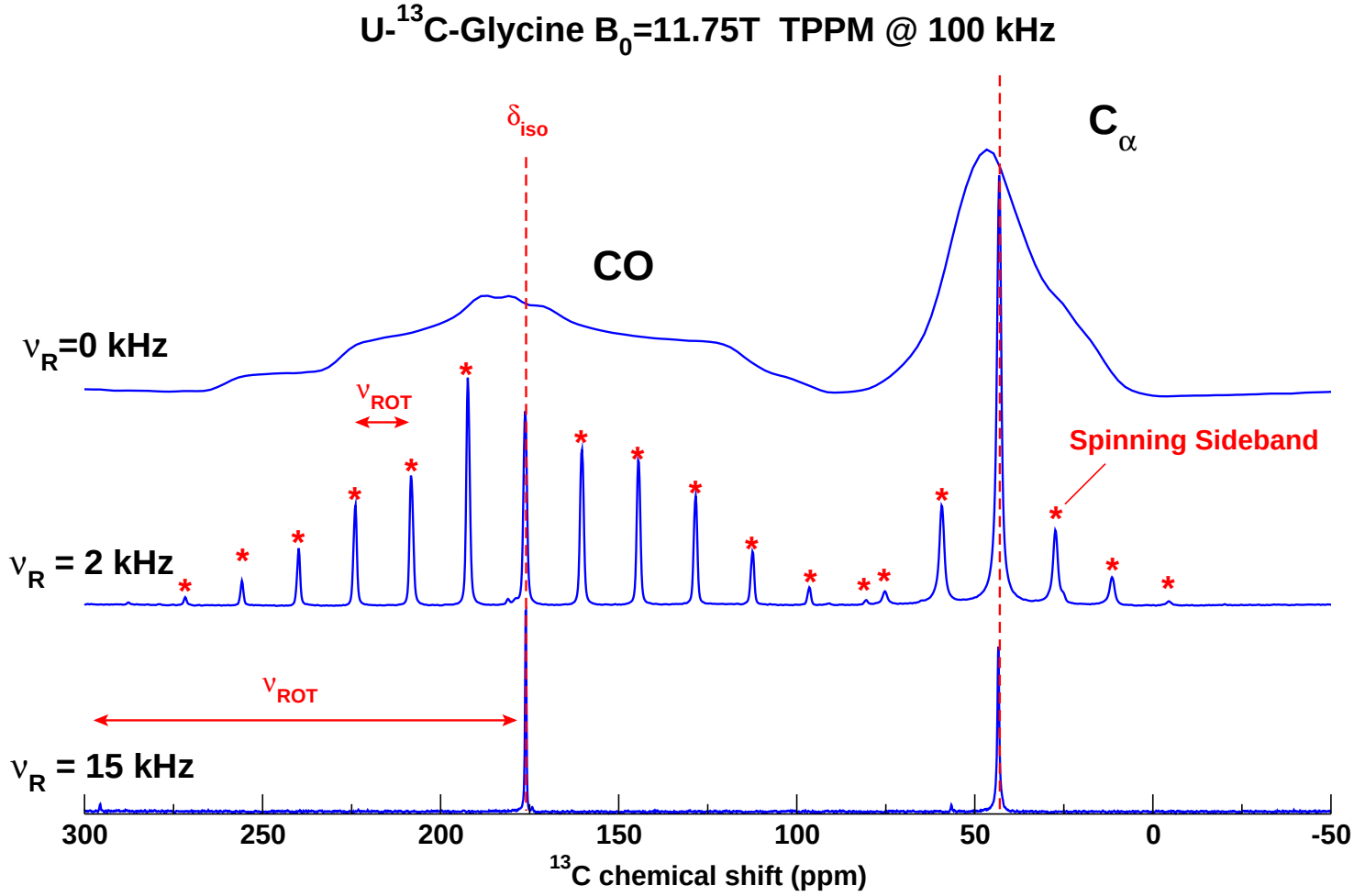

$\nu_{ROT} \leq \delta_A$: spinning sidebands at $k \times \nu_{ROT}$

$\nu_{ROT} > \delta_A$: narrow lines

(Experimental) Solid State NMR

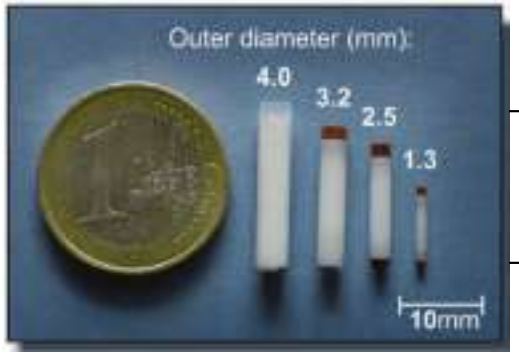

^{29}Si MAS NMR

$Q^{(n)}$: $Si(OSi)_n(O^-)_{(4-n)}$

^{29}Si MAS NMR:
Direct access to silicon $Q^{(n)}$ speciation

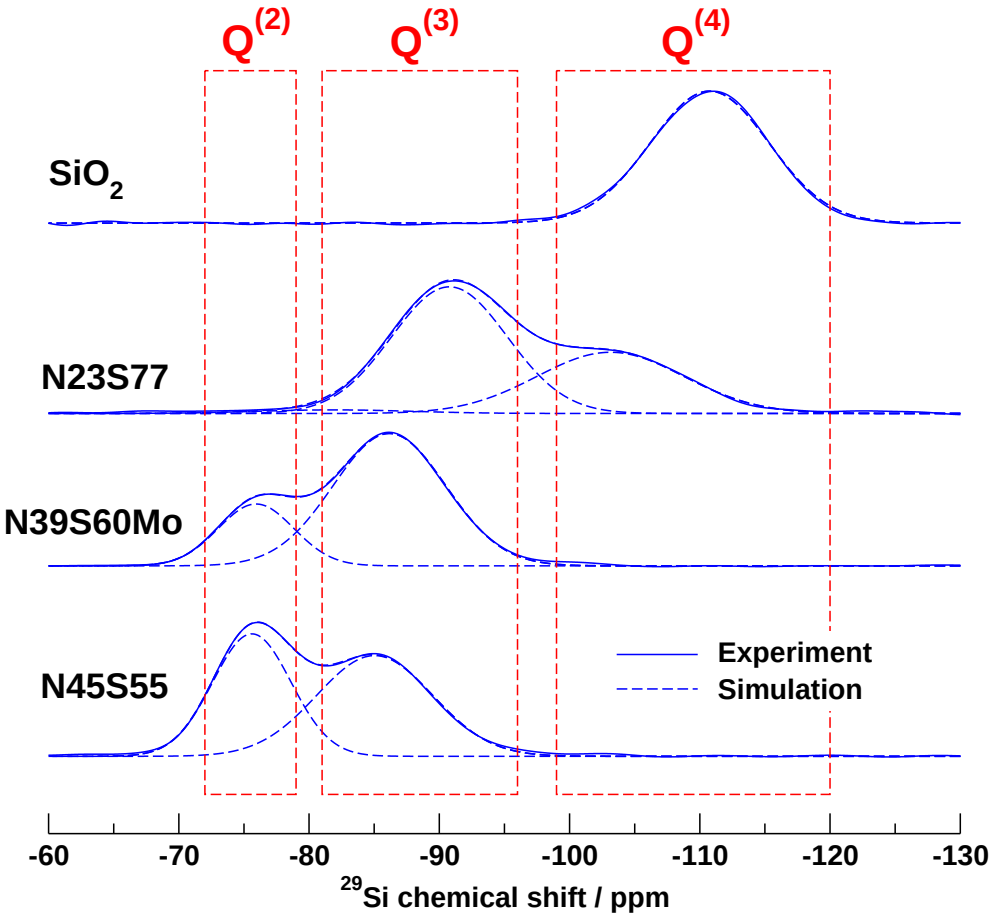

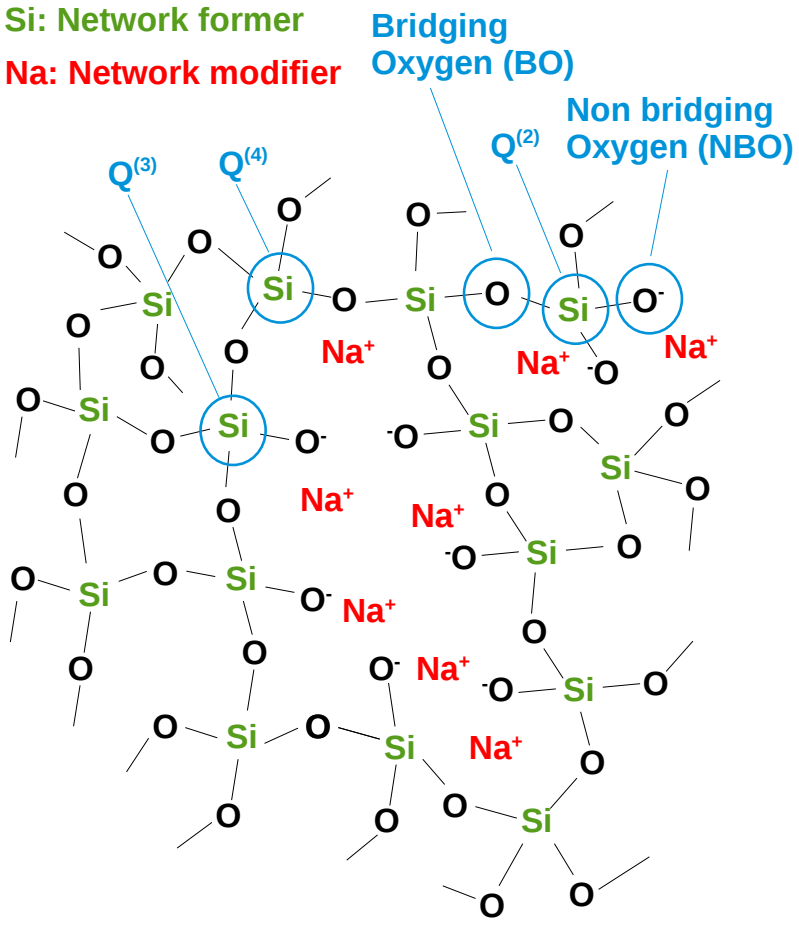

NMR peaks reflective of a Gaussian distribution of δ_{iso} (I=1/2)

Note: $\delta_{iso} = -(\sigma_{ref} - \sigma_{iso})$

The magnetic shielding

Relationshield with the chemical environment

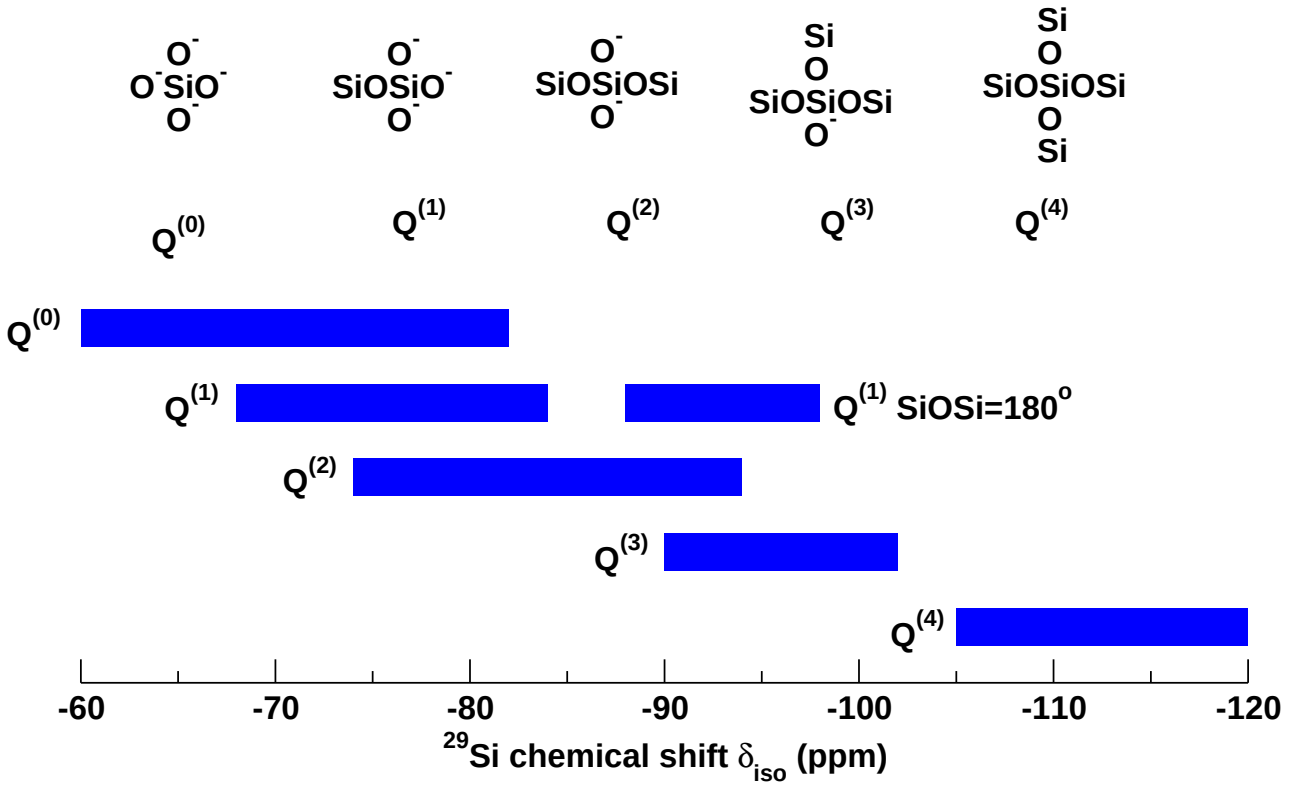

Tetrahedral silicon $Q^{(n)}$ units in crystalline silicates

High Resolution NMR

Magic Angle Spinning for quadrupolar nuclei: The central transition

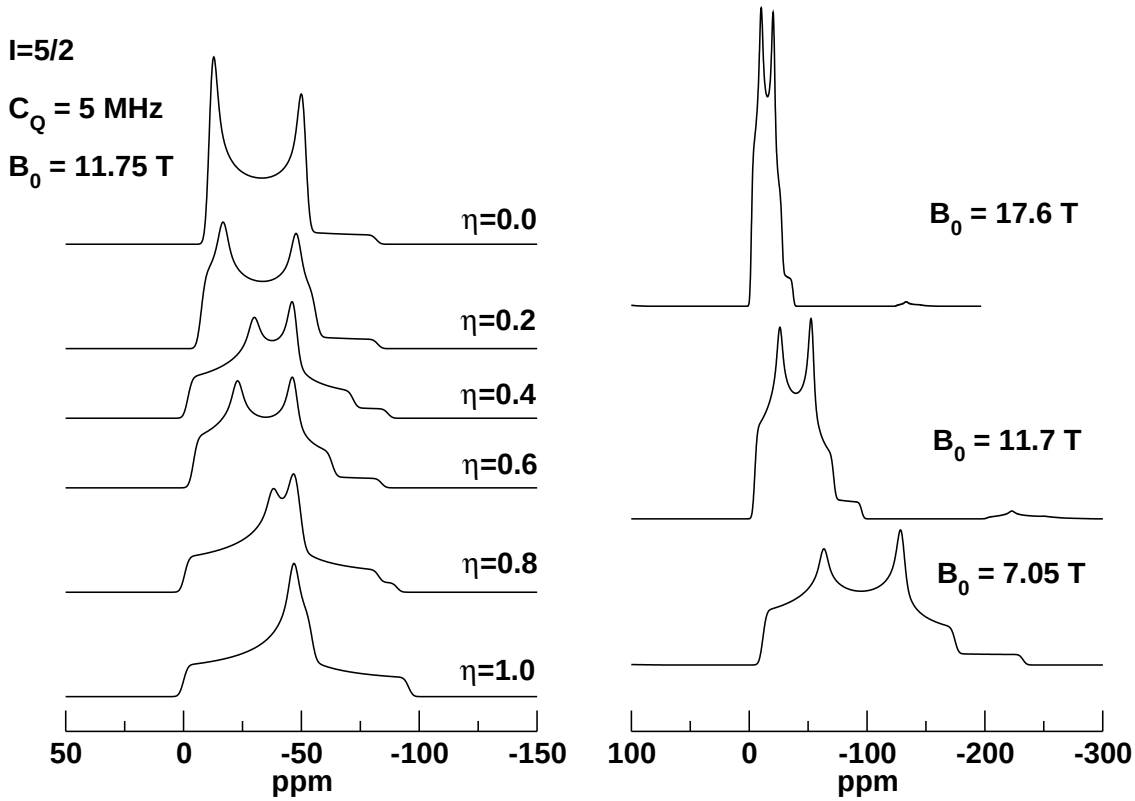

Second order decreases with the field: $H_Q^{(2)} \propto \nu_0^{-1}$

High Resolution NMR of quadruplar nuclei

Magic Angle Spinning for quadruplar nuclei: The satellite transitions

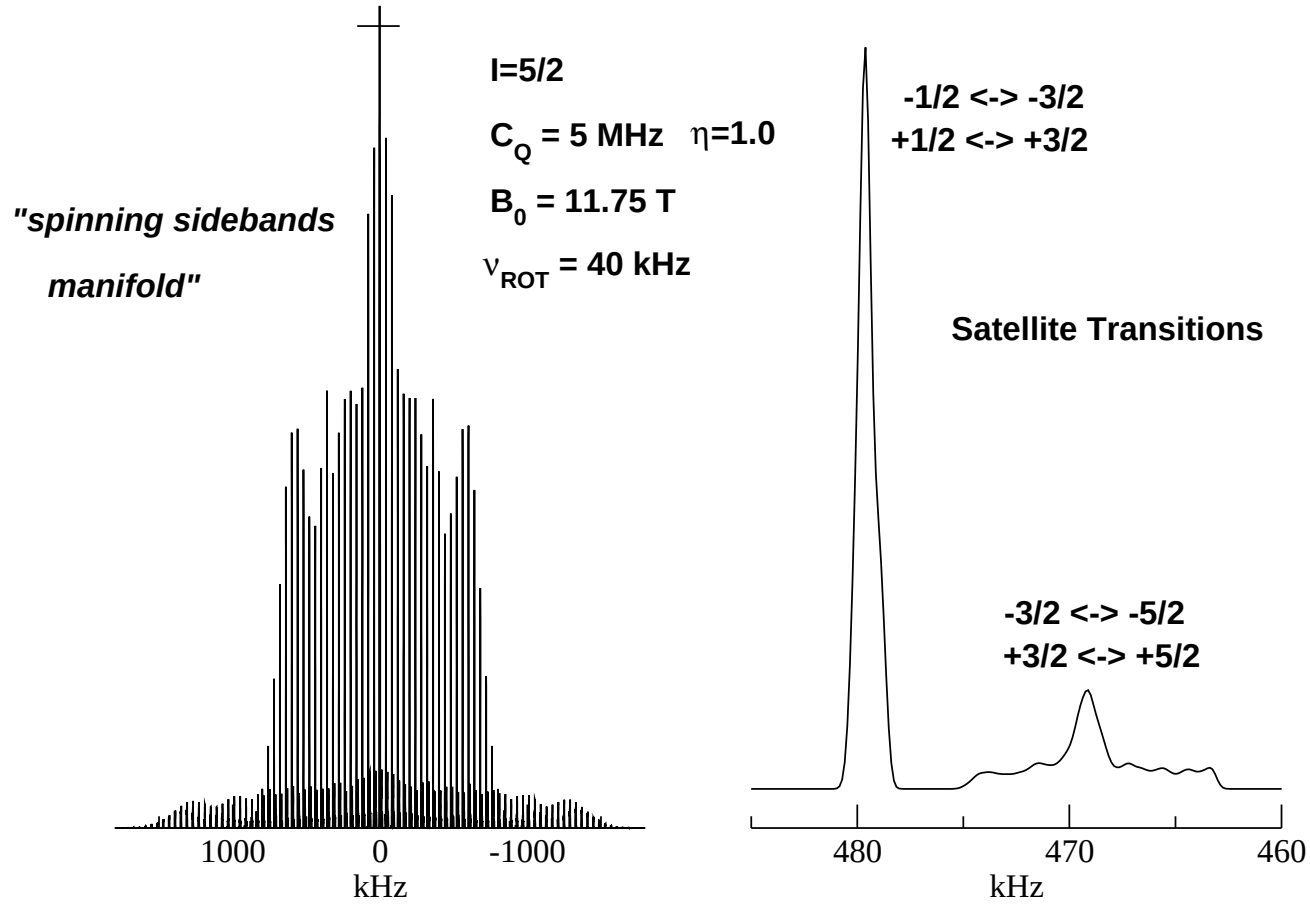

High Resolution NMR of quadrupolar nuclei

How to reduce the linewidth ?

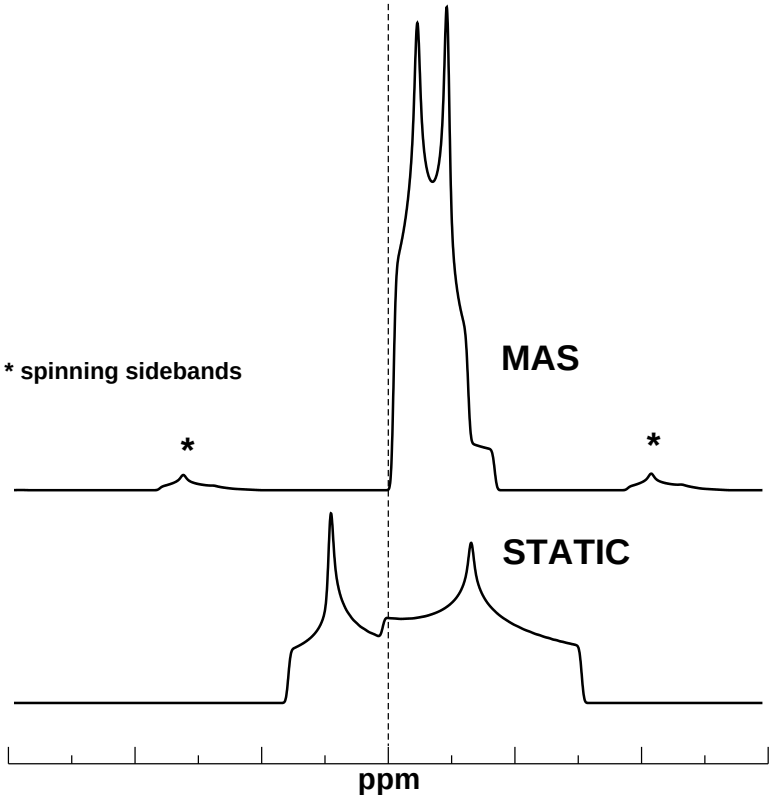

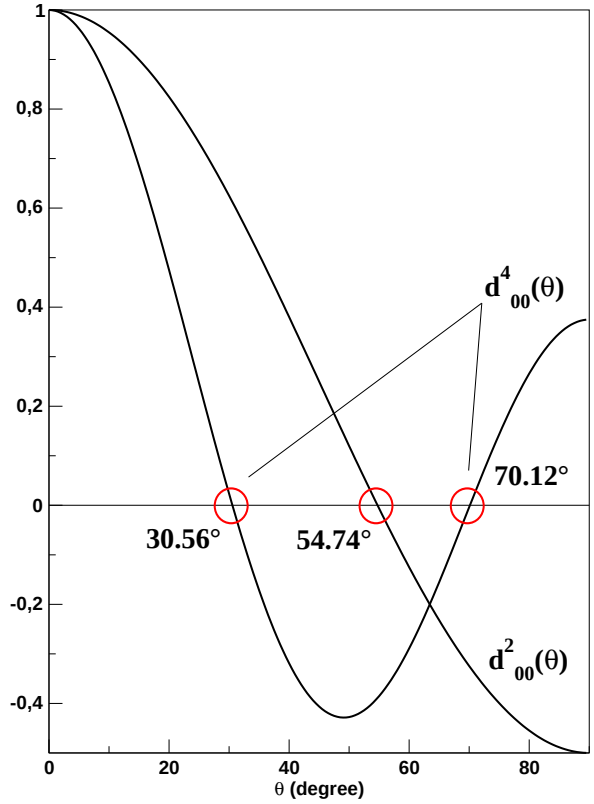

$$\text{static: } \nu_{CT} = \nu_{iso} + a_2 R_{20}^{(s)}(\Omega) + a_4 R_{40}^{(s)}(\Omega)$$

$$\text{MAS: } \nu_{CT} = \nu_{iso} + a_4 R_{40}^{(MAS)}(\Omega)$$

Fourth rank anisotropies not removed (*averaged out*) by MAS.

High Resolution NMR of quadrupolar nuclei

The Multiple Quantum MAS (MQMAS) approach: 2D NMR

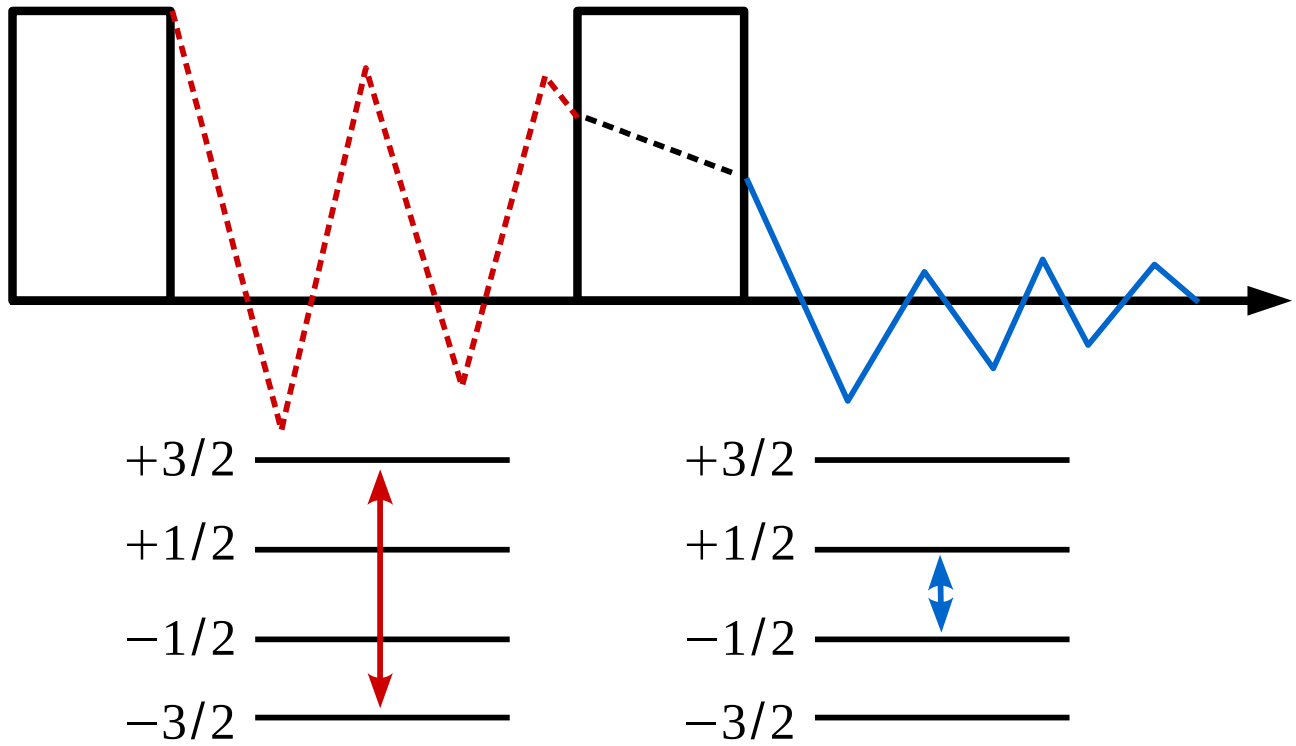

2D NMR: $S(t_1, t_2) = \exp\{-i\,\nu_{3Q}\,t_1\} \times \exp\{-i\,\nu_{1Q}\,t_2\}$

2D FFT yields a 2D spectrum $S(\nu_1, \nu_2)$

High Resolution NMR of quadrupolar nuclei

Principles of MQMAS NMR

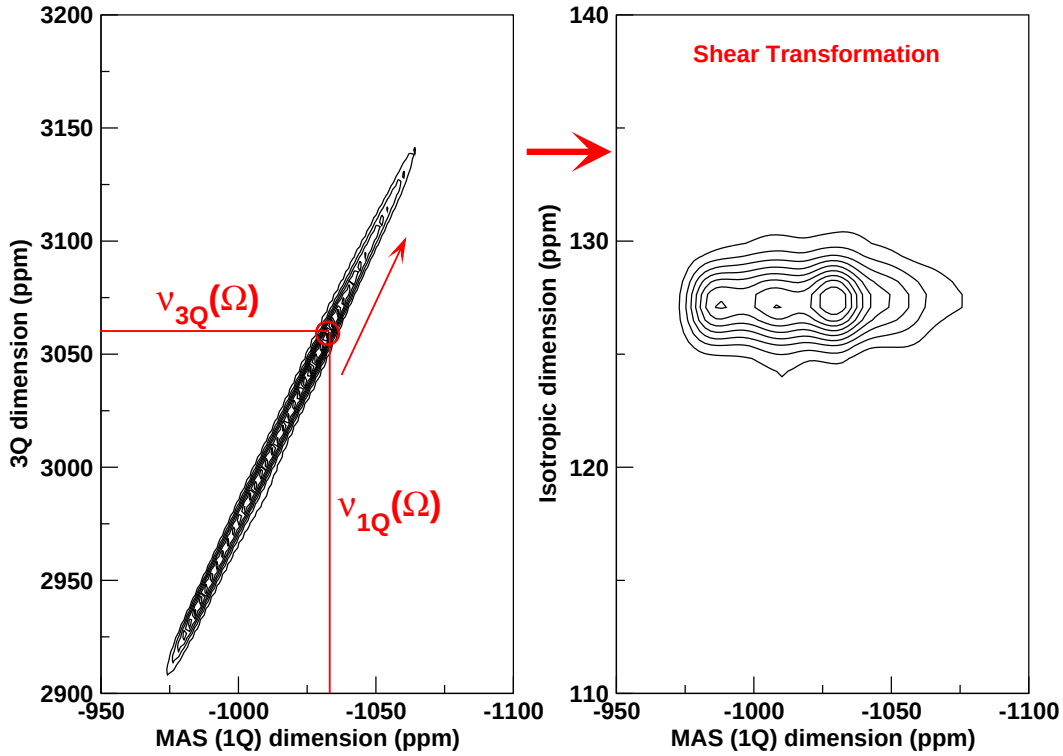

Both transitions *share* the same (4^{th} rank) anisotropic factor !

$$\nu_{(1Q=CT)} = \nu_{iso}^{(1Q)} + a_4(1Q)\, R_{40}^{(MAS)}(\Omega)$$

$$\nu_{(3Q=TQ)} = \nu_{iso}^{(3Q)} + a_4(3Q)\, R_{40}^{(MAS)}(\Omega)$$

High Resolution NMR of quadrupolar nuclei

MQMAS at work in a crystalline sample

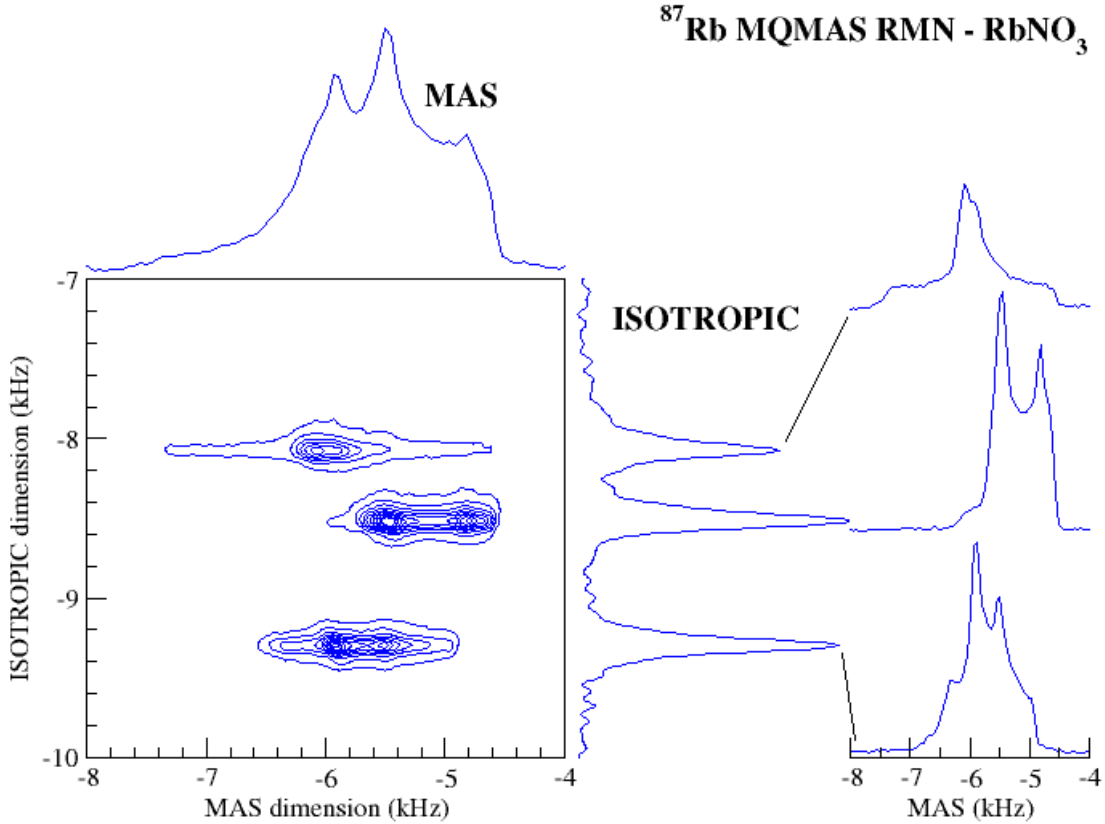

Solid State NMR of disordered materials

MAS NMR: mechanisms of broadening?

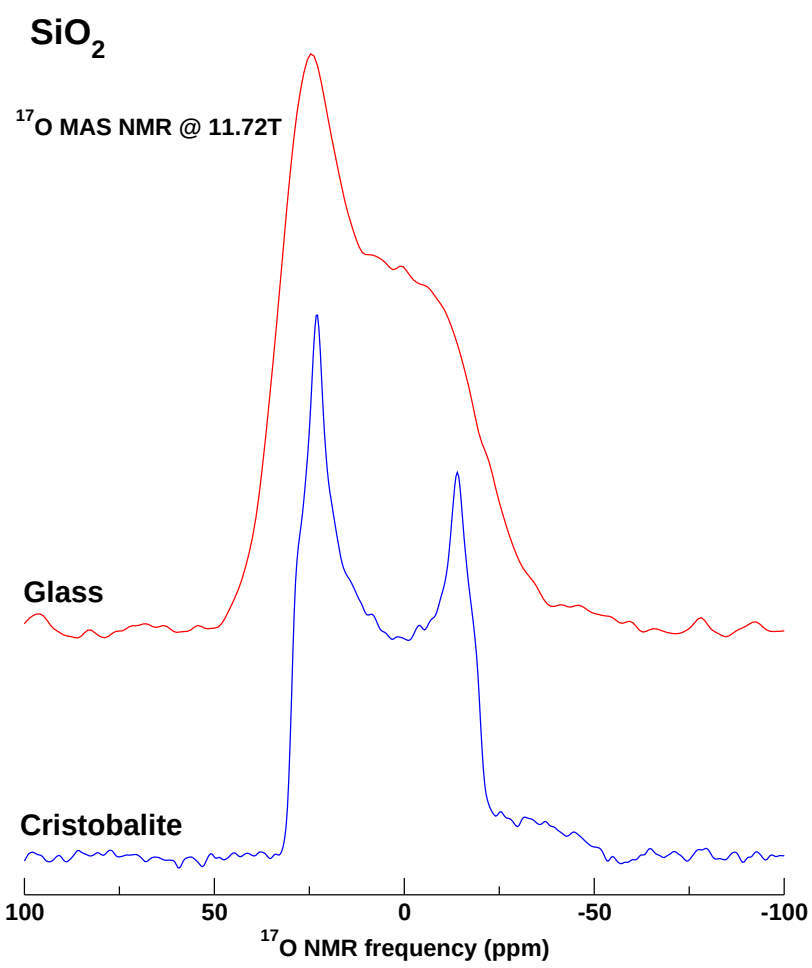

Cristobalite D. Neuville (IPGP)

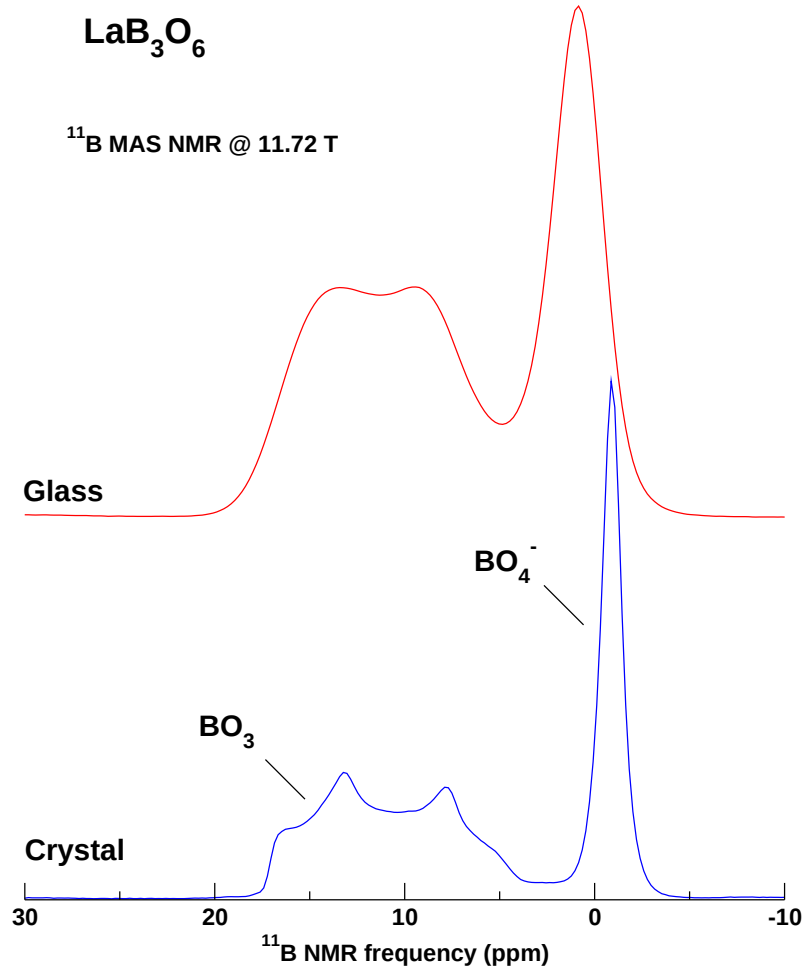

Sample. H. Tregouet, D Caurant (ENSCP)

Need of 2D NMR to elucidate the contribution of EFG and chemical shift distribution.

Solid State NMR of disordered versus crystalline materials

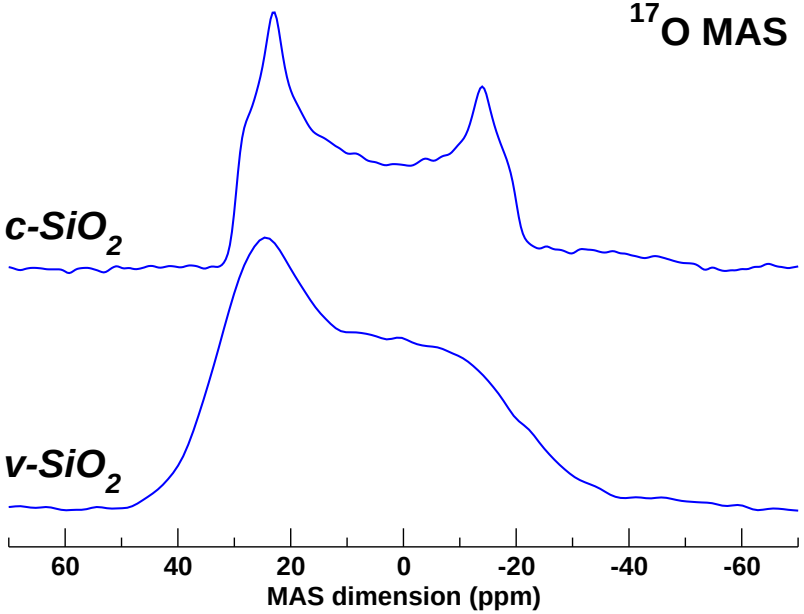

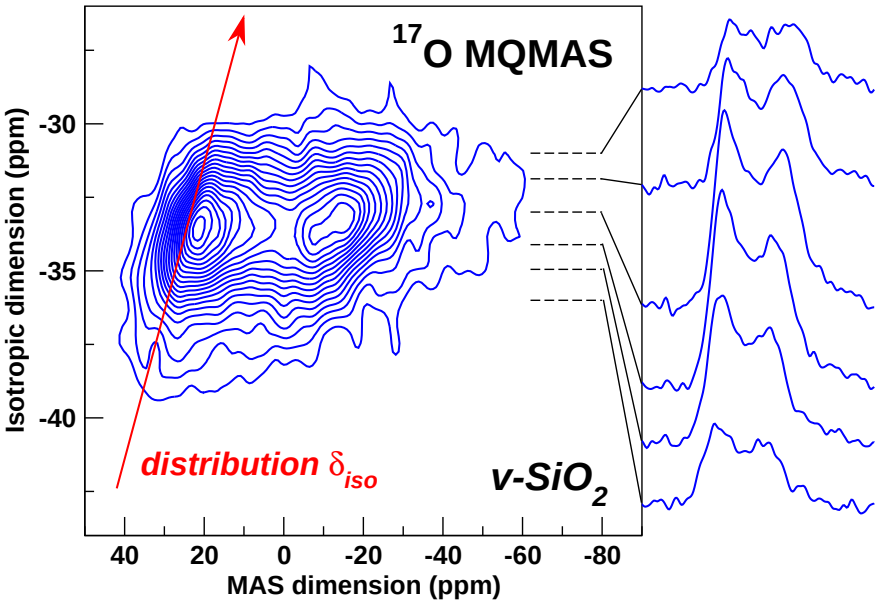

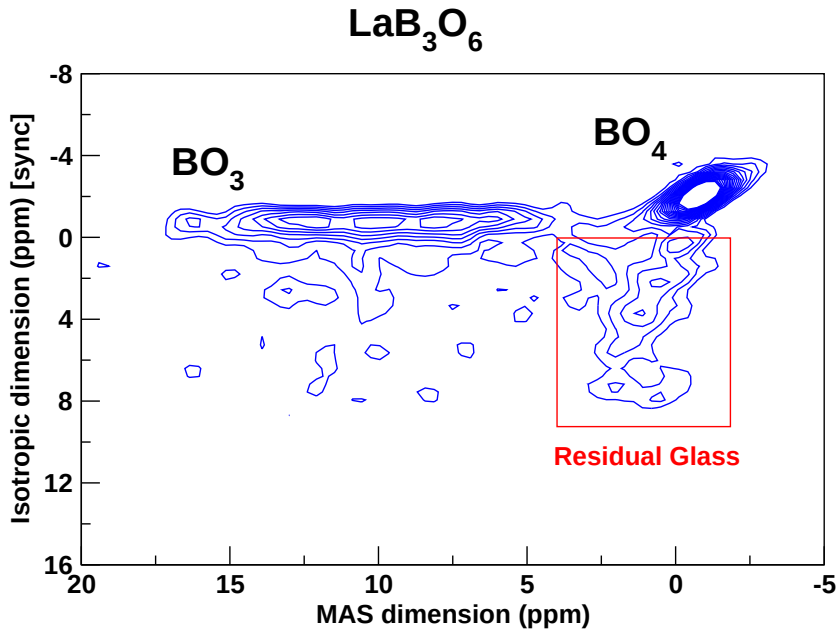

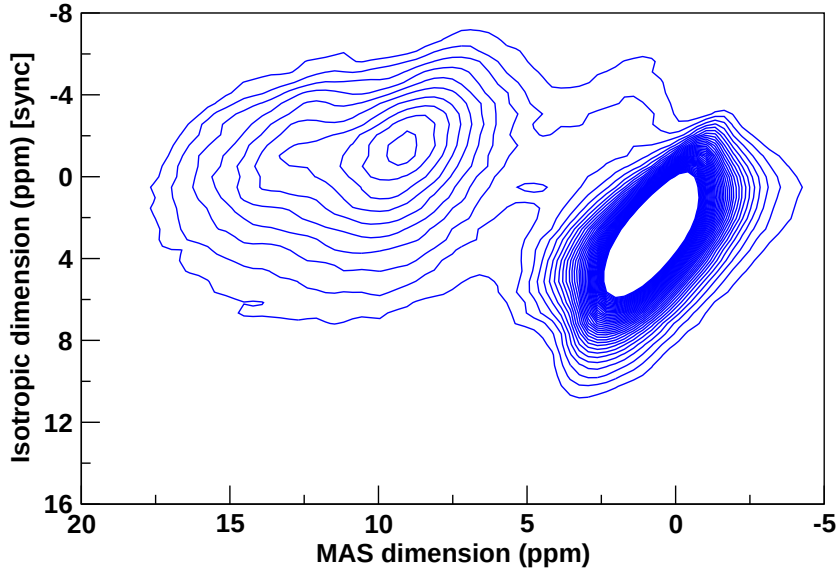

Coll. H. Tregouet, D. Caurant (ENSCP)

^{17}O and ^{23}Na MAS NMR

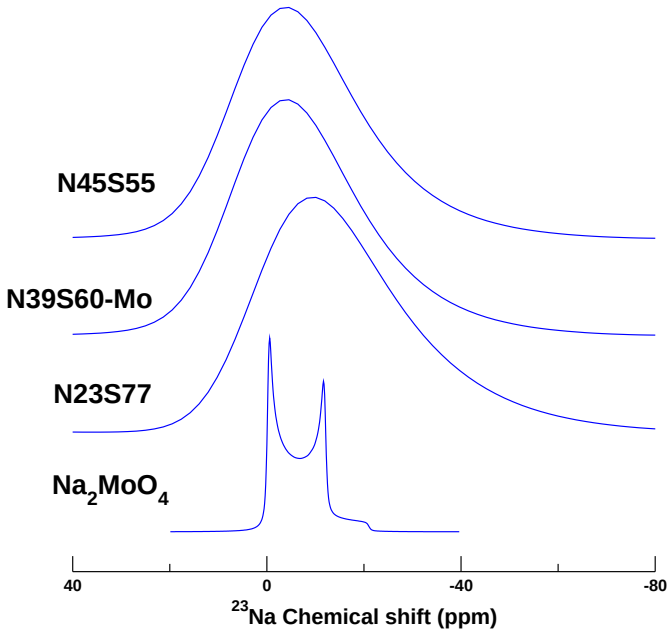

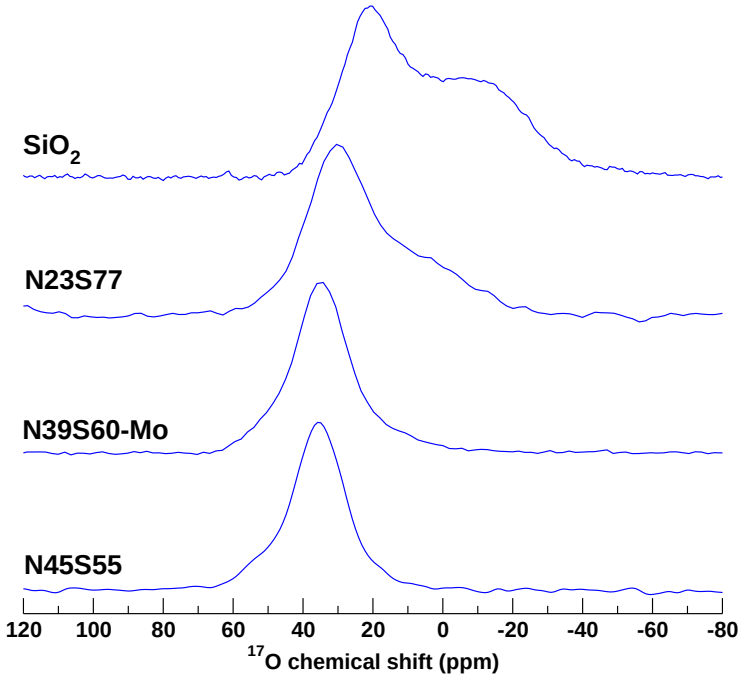

- ^{17}O NMR parameters, nuclear spin $I = 5/2$ (^{23}Na $I = 3/2$)
  - Isotropic chemical shift δ_{iso}
  - Quadrupolar coupling constant C_Q, asymmetry η ($I > 1/2$)
- Disordered solids:
  $\Rightarrow$ NMR parameter distribution $p(\delta_{iso}, C_Q, \eta)$ needed but unknown

Coll. F. Angeli, S. Schuller CEA/DEN, Geochim. Cosmo. Acta 75 (2011)

MQMAS NMR with NMR parameter distribution

C_Q (Gaussian) distribution

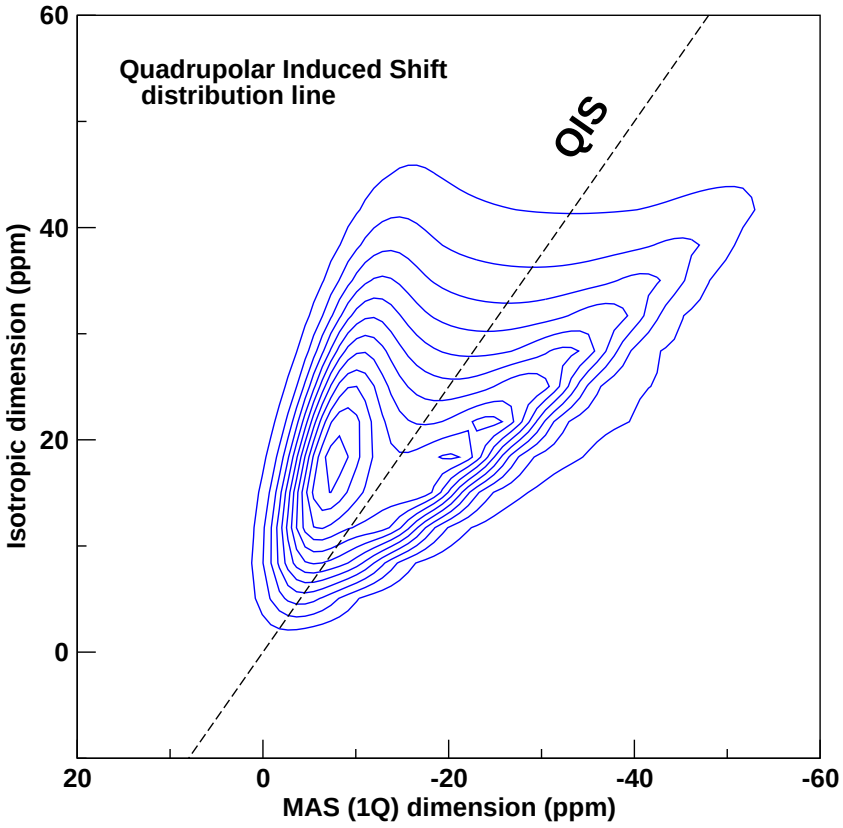

δ_{iso} (Gaussian) distribution

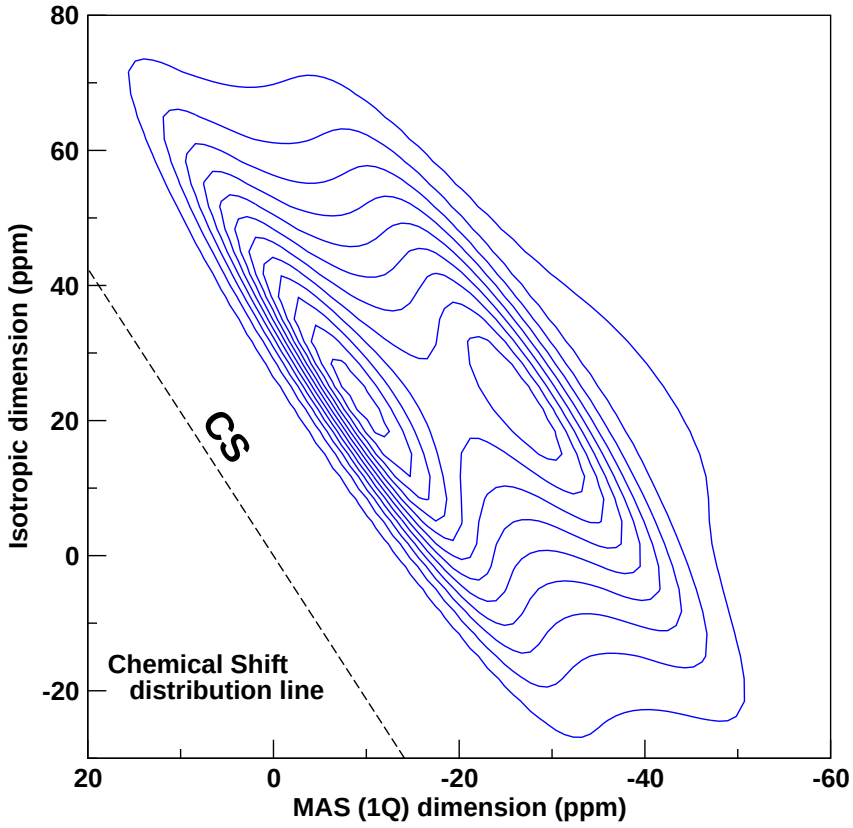

$\Rightarrow$ MQMAS NMR can *separate* C_Q and δ_{iso} distribution

^{23}Na MQMAS NMR

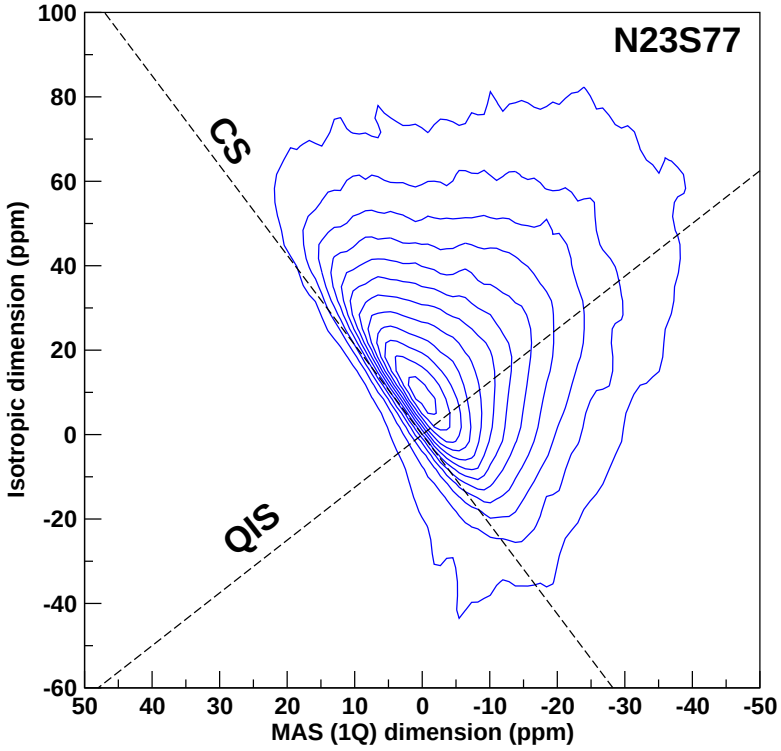

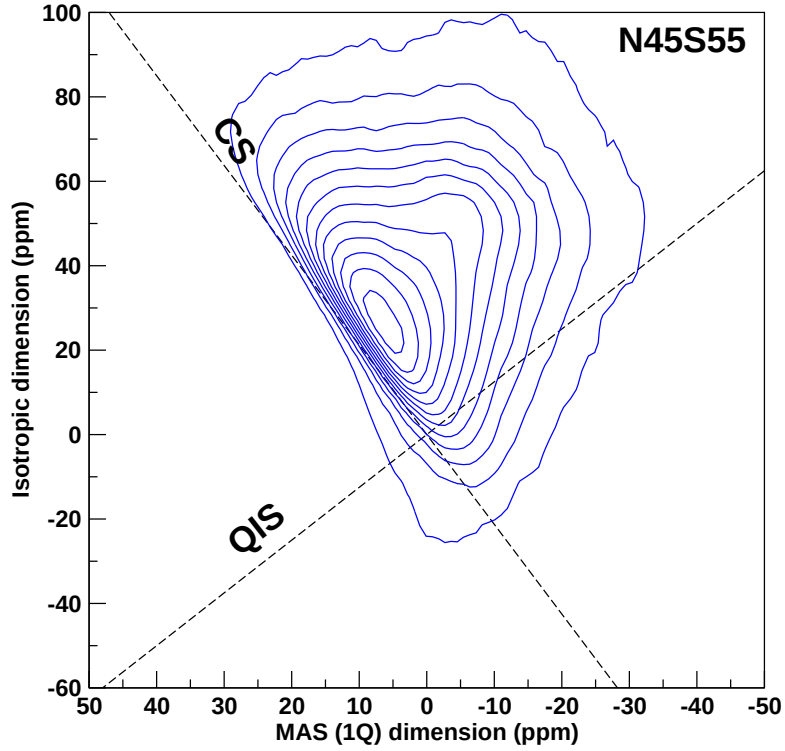

- Broad distribution: highly disordered environment (ionic int.)
- What is the underlying $p(\delta_{iso}, C_Q, \eta)$ (analytical expression)
- How do we fit / process the data ?

The power of ^{17}O MQMAS Spectroscopy

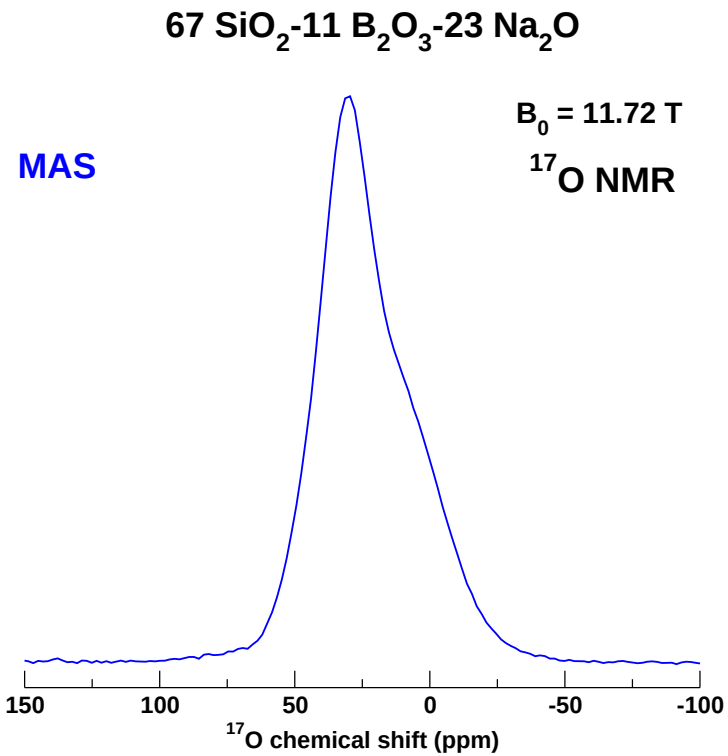

- MAS (1D): Unresolved

The power of ^{17}O MQMAS Spectroscopy

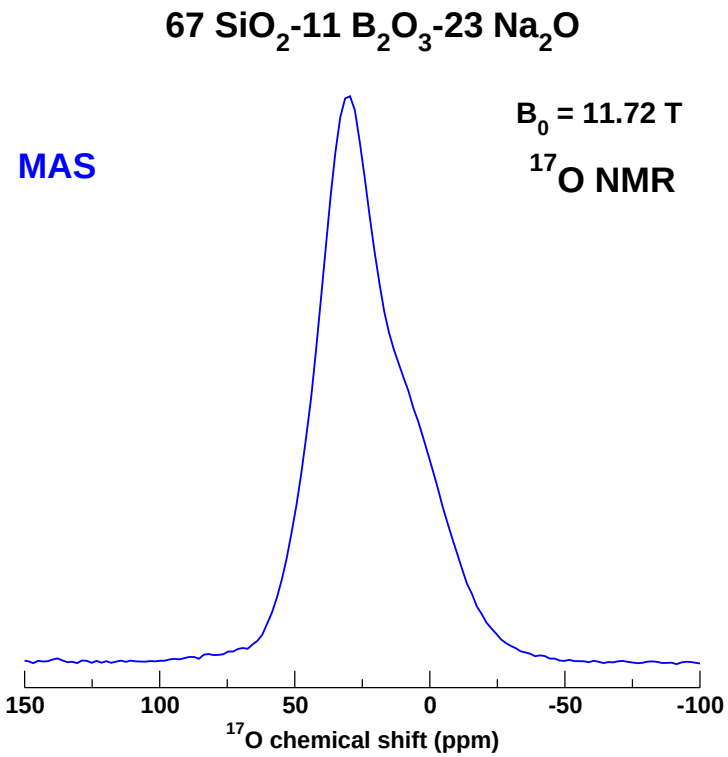

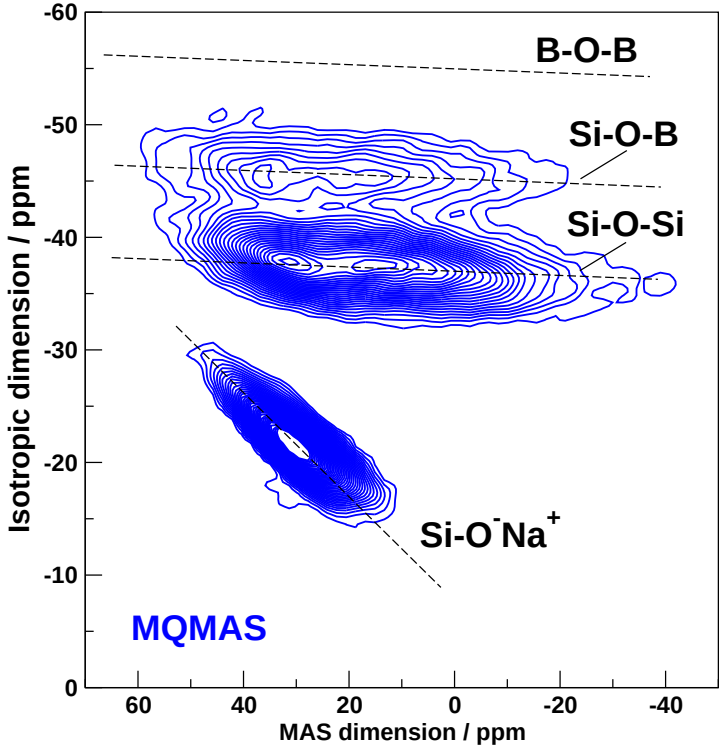

- MAS (1D): Unresolved
- MQMAS (2D): *Direct* reading the glass network structure

Structure of Soda-Lime Borosilicate Glasses.

The ^{17}O NMR approach

$67\ SiO_2$ - $11\ B_2O_3$
$22\ Na_2O$

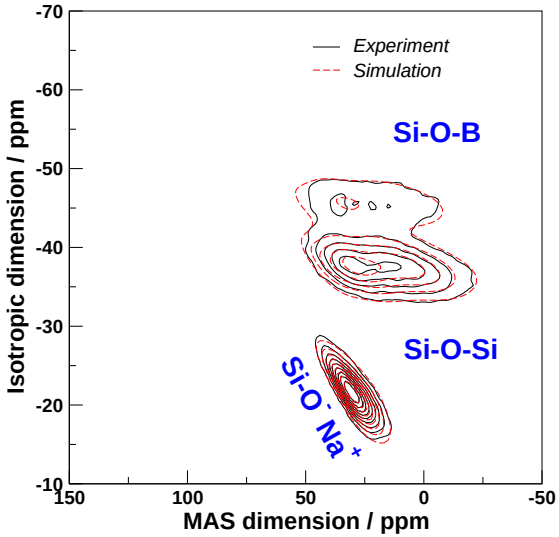

$67\ SiO_2$ - $11\ B_2O_3$
$16.5\ Na_2O + 5.5\ CaO$

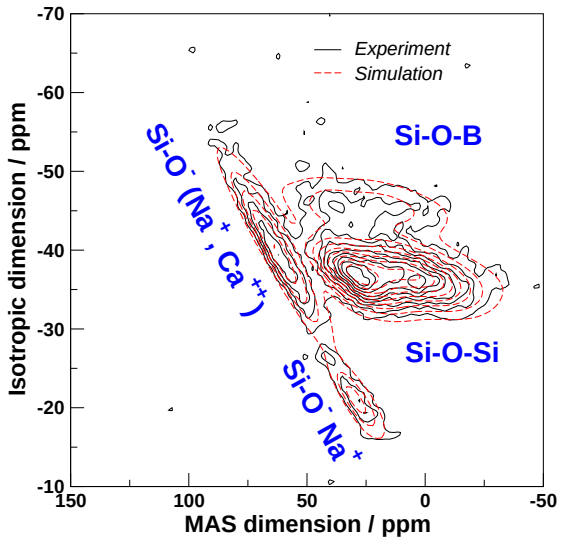

$67\ SiO_2$ - $11\ B_2O_3$
$11\ Na_2O + 11\ CaO$

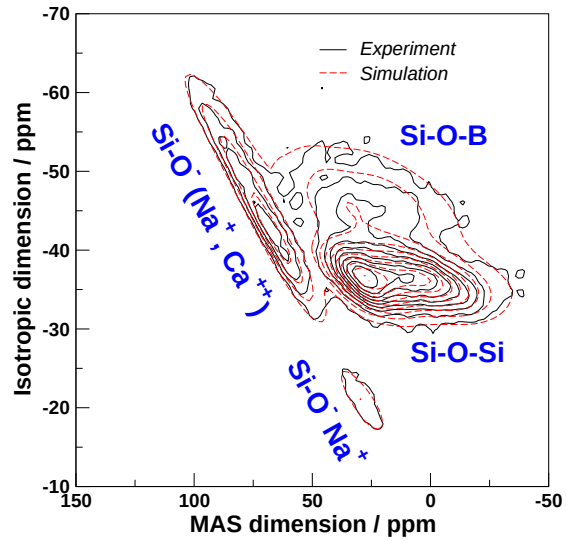

$\Rightarrow$ Quantification of the Na/Ca mixing.

$\Rightarrow$ Network structure, Si/B mixing.

Coll. F. Angeli CEA/DEN

Oxygen-17 MQMAS NMR

60.4 SiO_2 - 15.3 B_2O_3 - 19 Na_2O - 5.2 CaO

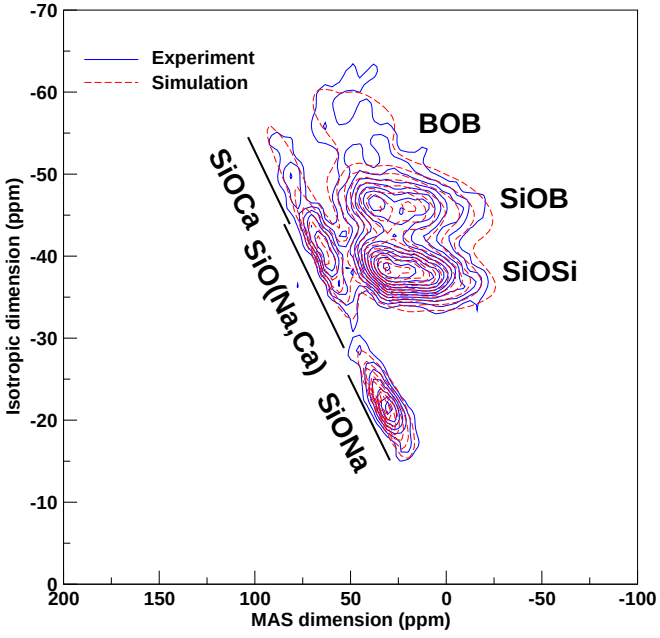

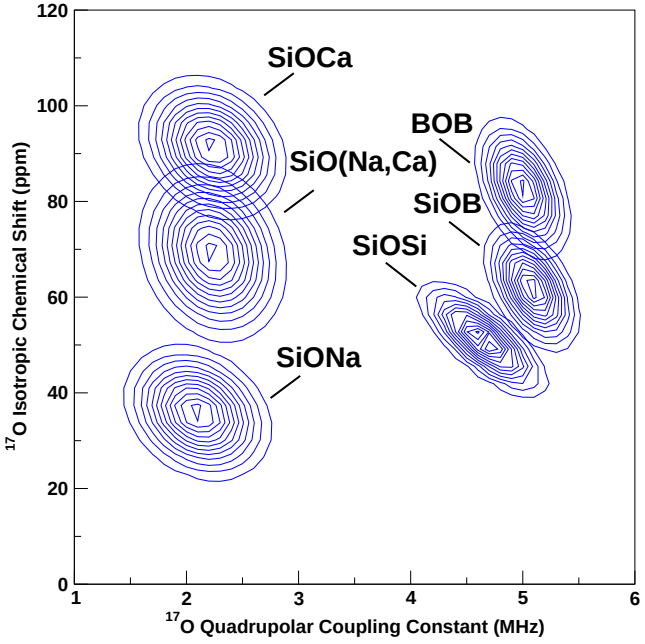

Si/B random mixing

	Theory	^{17}O
Si-O-Si	34.1	35.6
Si-O-B	42.1	42.8
B-O-B	13.0	11.3
NBO	10.8	10.2

- Data in agreement with Si/B random mixing
- Evidence of Na/Ca mixing in depolymerized regions (DR)
- Ca is modifier (^{11}B NMR: $BO_4^- \rightarrow BO_3$)

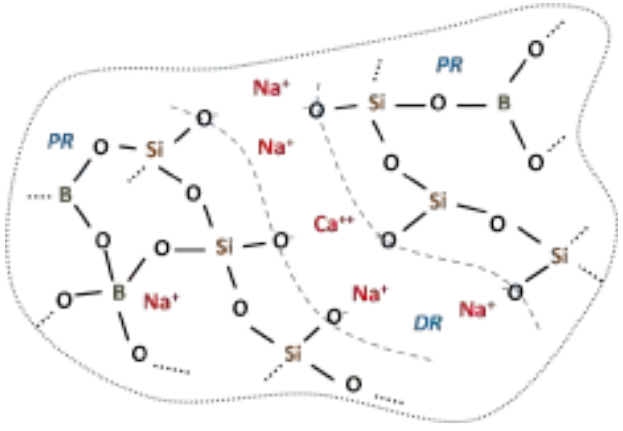

J. Am. Ceram. Soc **93** 2010; J. Non Cryst. Solids **354** 2008

Introducing DFT calculations in solid state NMR

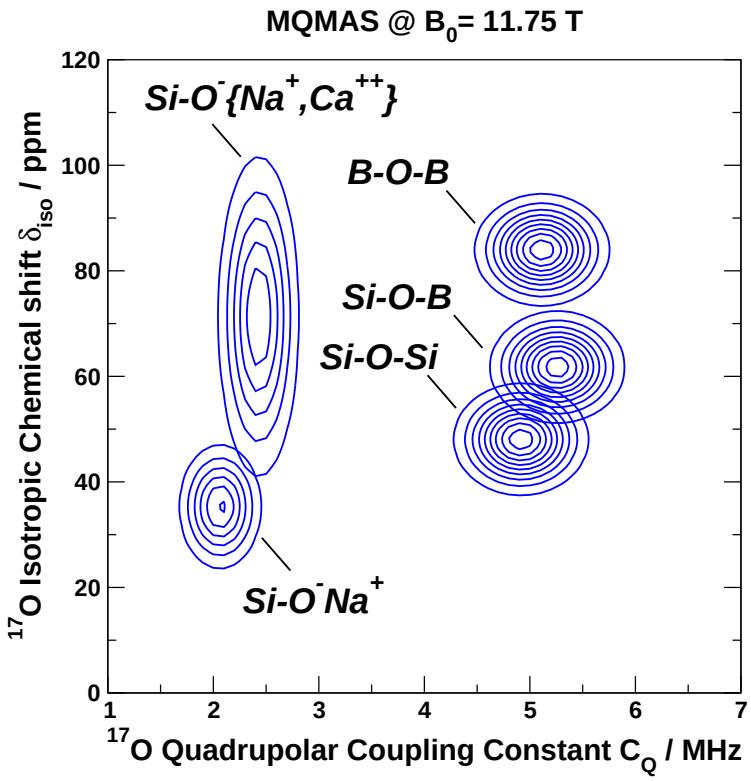

Glass Structure

- Reconstruction of the NMR parameter distribution
- Correlating the *local disorder* to the NMR spectrum line shape ?
- $\Pi(\text{NMR}) \Rightarrow \Pi(\text{Structure})$?
- Improve the interpretation of NMR data

Understanding NMR / Structure relationships

Quantum Mechanical calculations: the Cluster Approach

$Si(OH)_3$-O-$Si(OH)_3$

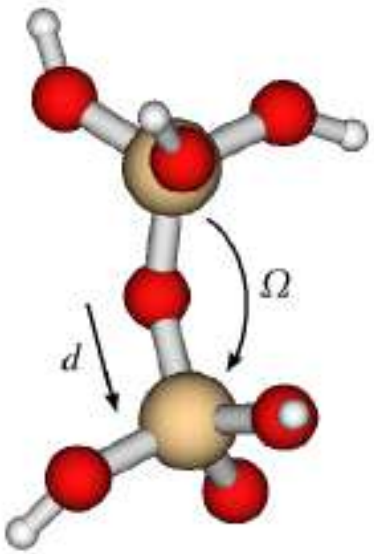

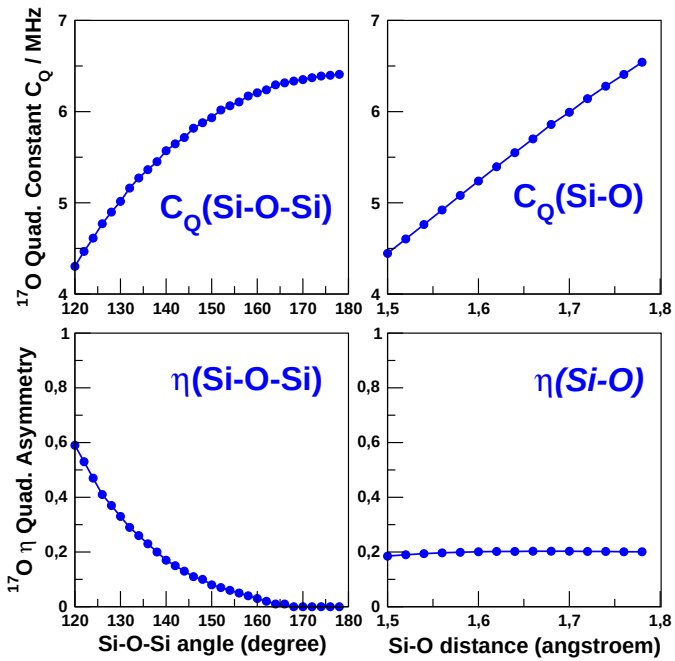

^{17}O C_Q and η_Q NMR parameters are allmost exclusively controlled by local properties: (Si-O-Si bond angle and Si-O bond length)

Combining MD simulations with DFT NMR calculations

MD + DFT GIPAW

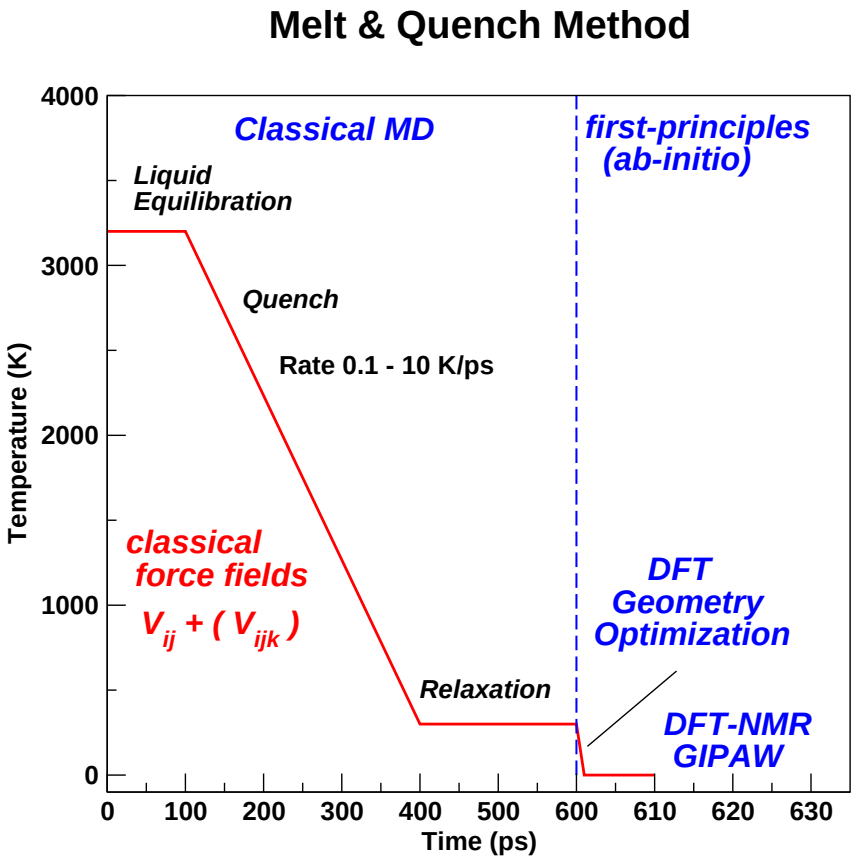

Gauge Including Projector Augmented Wave **GIPAW** C.J. Pickard & F. Mauri, PRB 2001

- Plane Wave pseudopotential DFT
- Outputs NMR interactions in crystallographic axes frame

$\Rightarrow$ First-Principles NMR (fpNMR)

Vitreous SiO_2

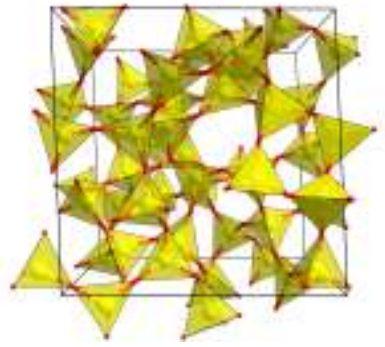

^{17}O *fp*NMR

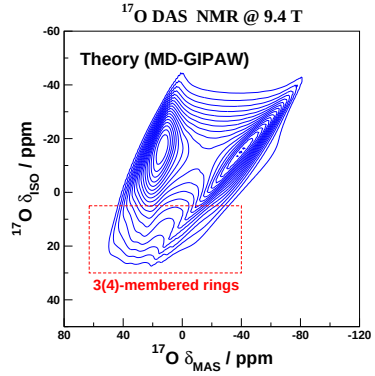

T. Charpentier et al, J. Phys. Chem. C 2009

Molecular Dynamics used for

$\Rightarrow$ Generating structural models, $\Rightarrow$ Effects of dynamics

Combining MD simulations with DFT NMR calculations

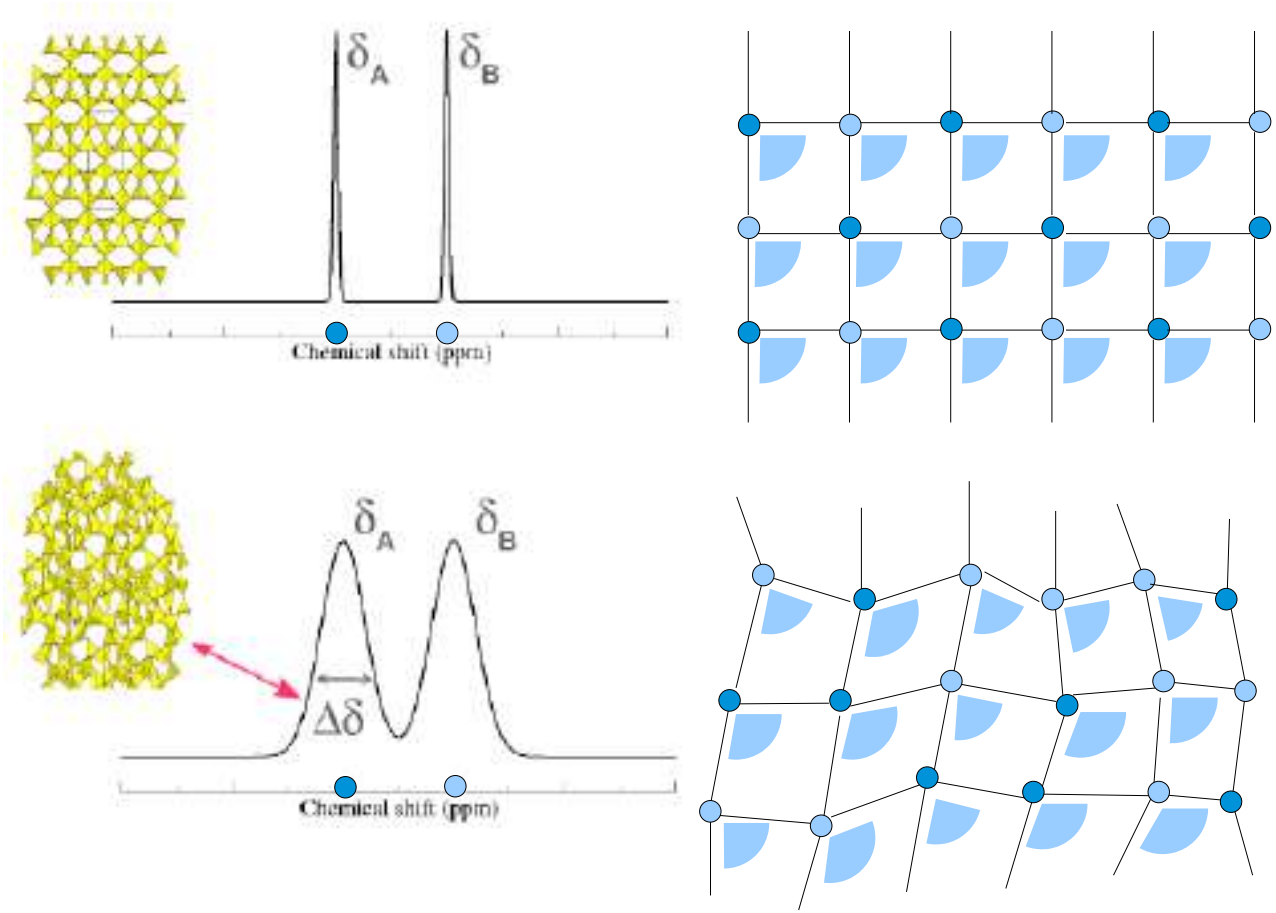

- MD simulations can (now) be compared to NMR experiments
- Effect of structural and chemical disorder on NMR
- NMR / structure (bond angle, distance, . . .) relationships

NMR driven choice of interaction potentials ($U_{ij}(r)$, ...)

NMR (now) offers new perspectives for assessing MD simulations (^{29}Si MAS NMR)

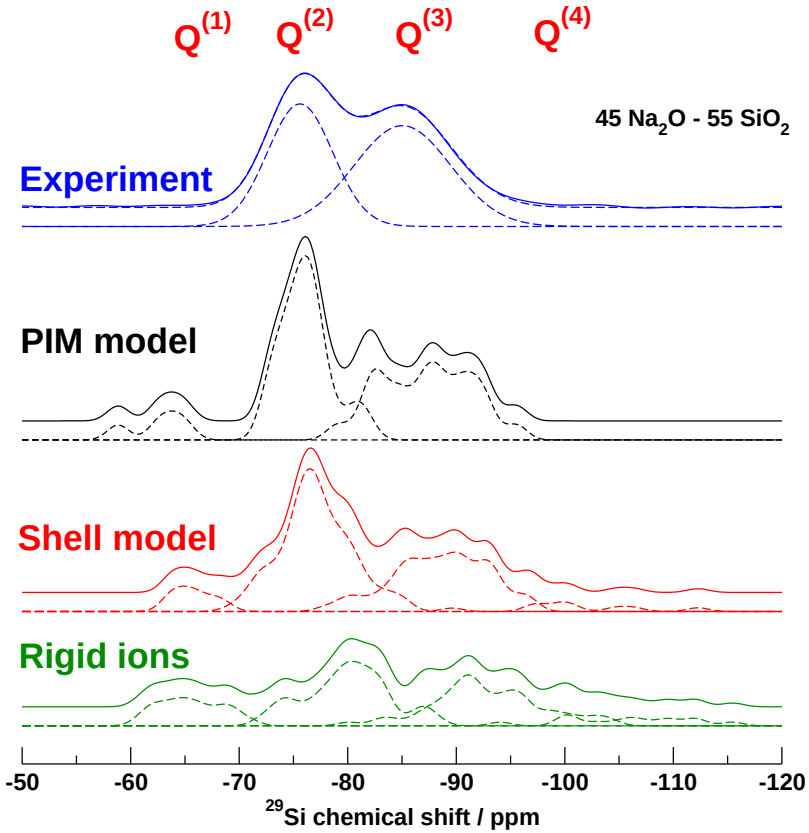

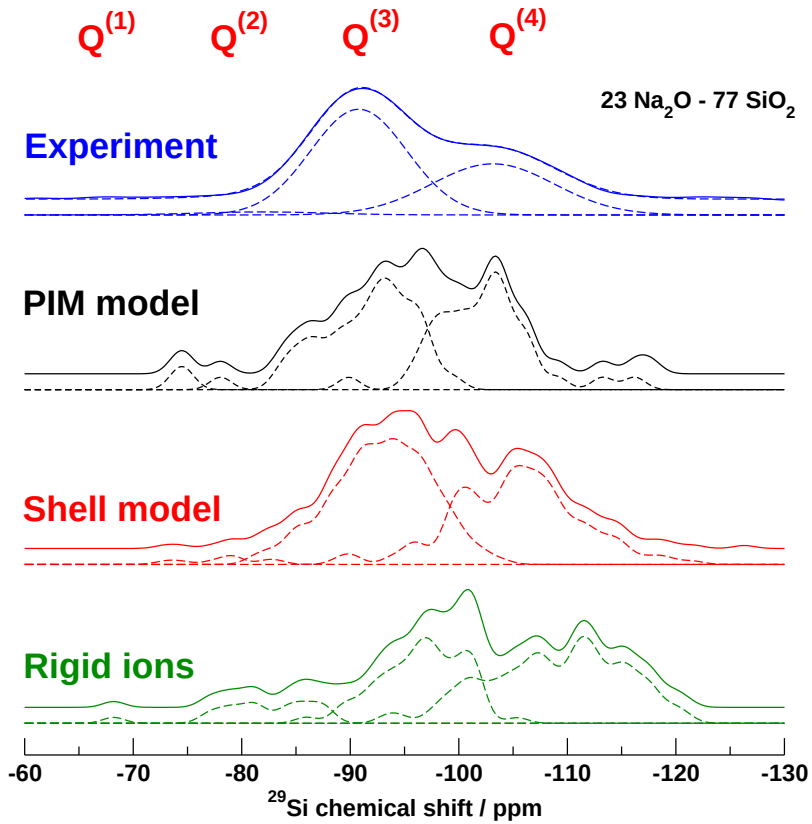

- Shell model: $O^{2-} = O^{(-2-Y)}_{core}$-$O^{(Y)}_{shell}$: ($Y = -2.8482$ e)
- PIM: q_i (rigid ions) + $\mu_i(t)$ Polarisability (O^{2-})
- Improved silicate network prediction ($Q^{(n)}$) with PIM

^{29}Si MAS NMR: Direct access to silicon $Q^{(n)}$ speciation

$Q^{(n)}$: $Si(OSi)_n(O^-)_{(4-n)}$

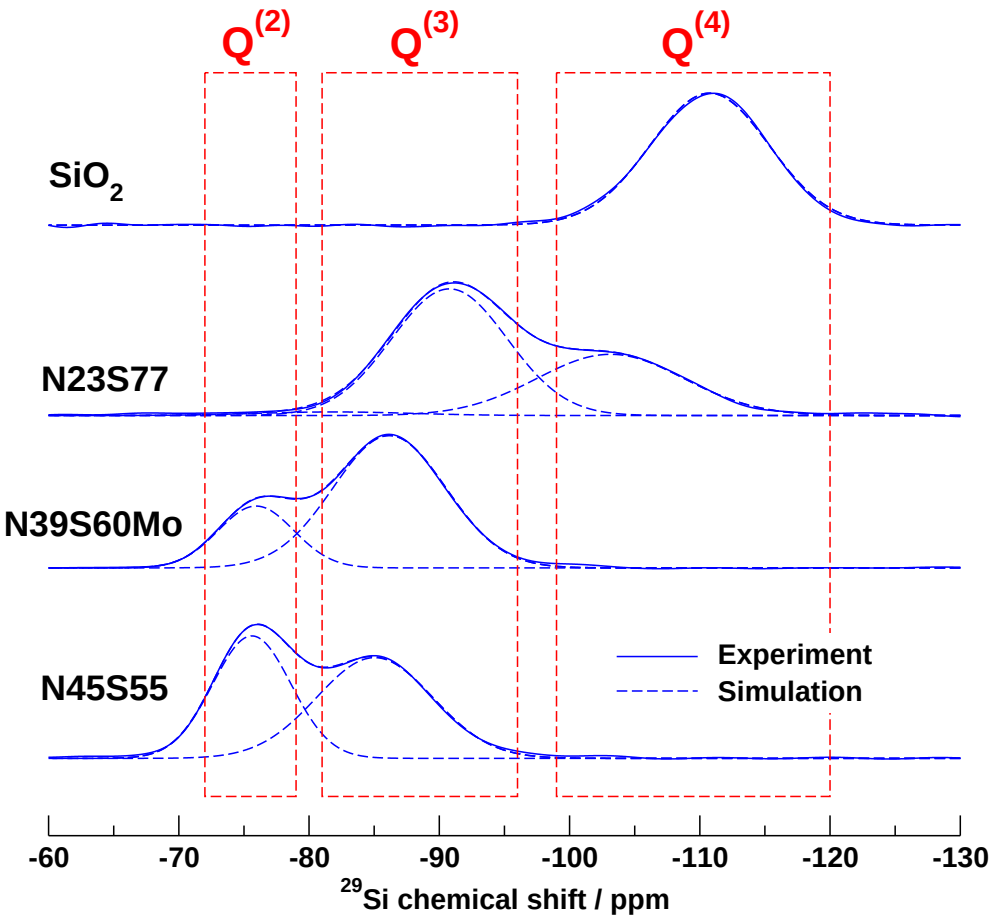

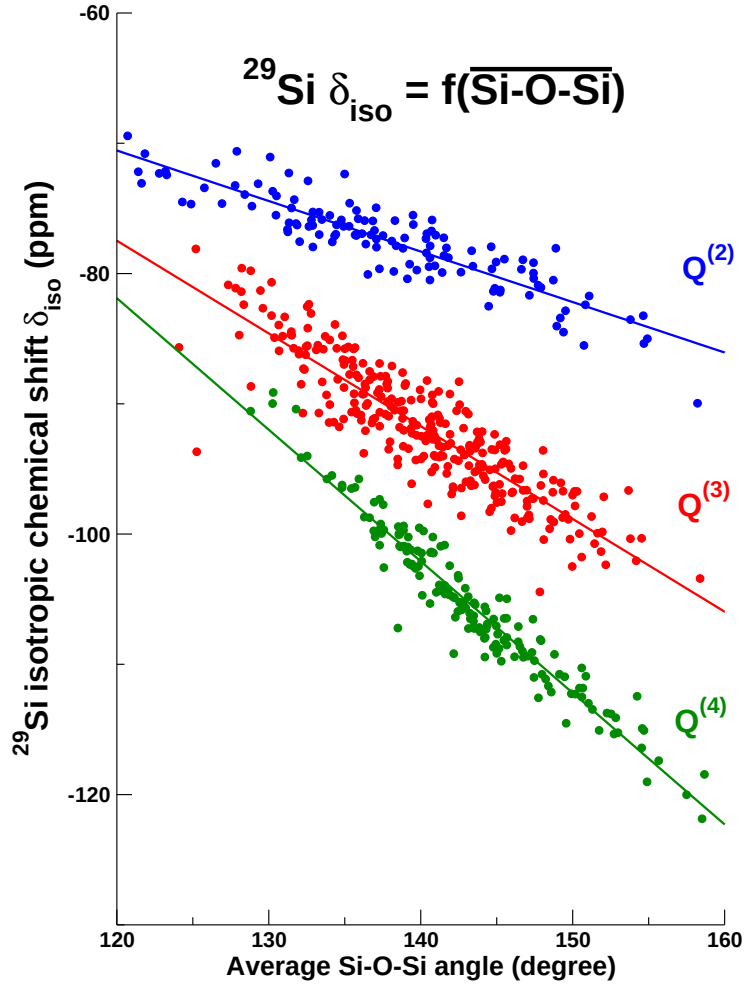

Binary Na_2O - SiO_2 glasses
NSMo: N39S60 + 1 MoO_3

The NMR response of $Q^{(n)}$ species to disorder (bond angle distribution) is different.

^{29}Si MAS NMR: Direct access to silicon $Q^{(n)}$ speciation

$Q^{(n)}$: $Si(OSi)_n(O^-)_{(4-n)}$

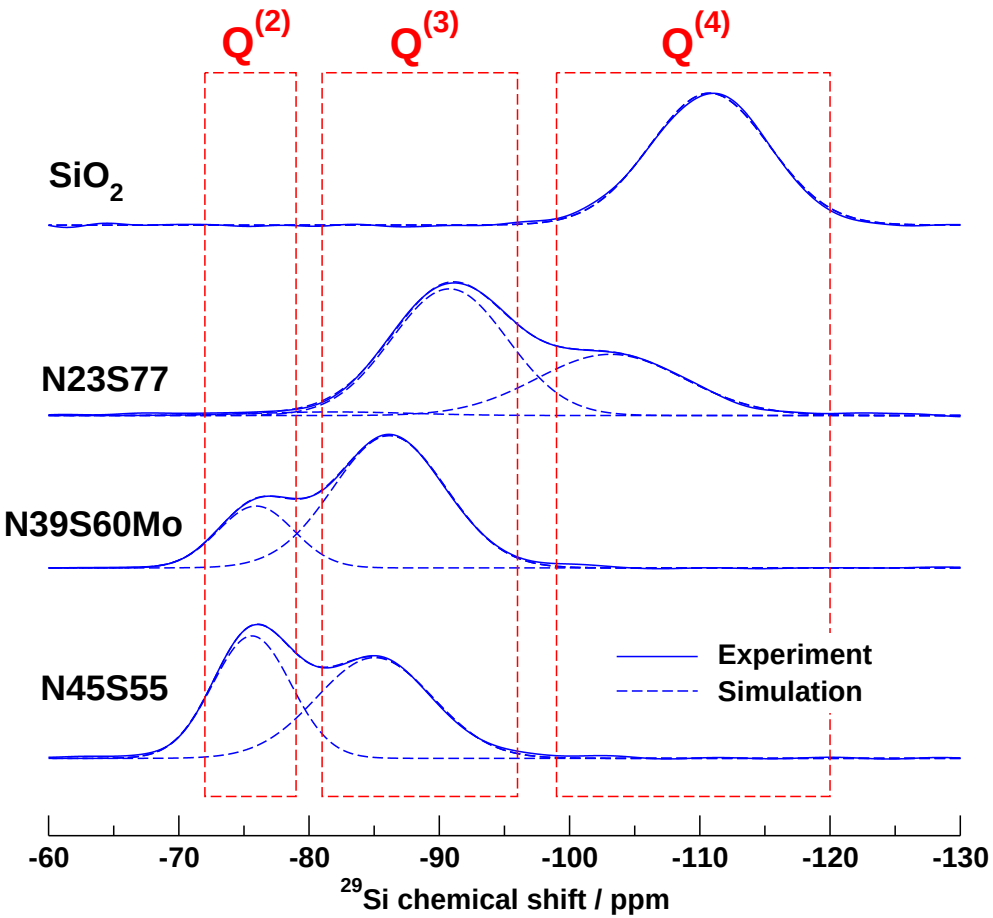

Binary Na_2O - SiO_2 glasses
NSMo: N39S60 + 1 MoO_3

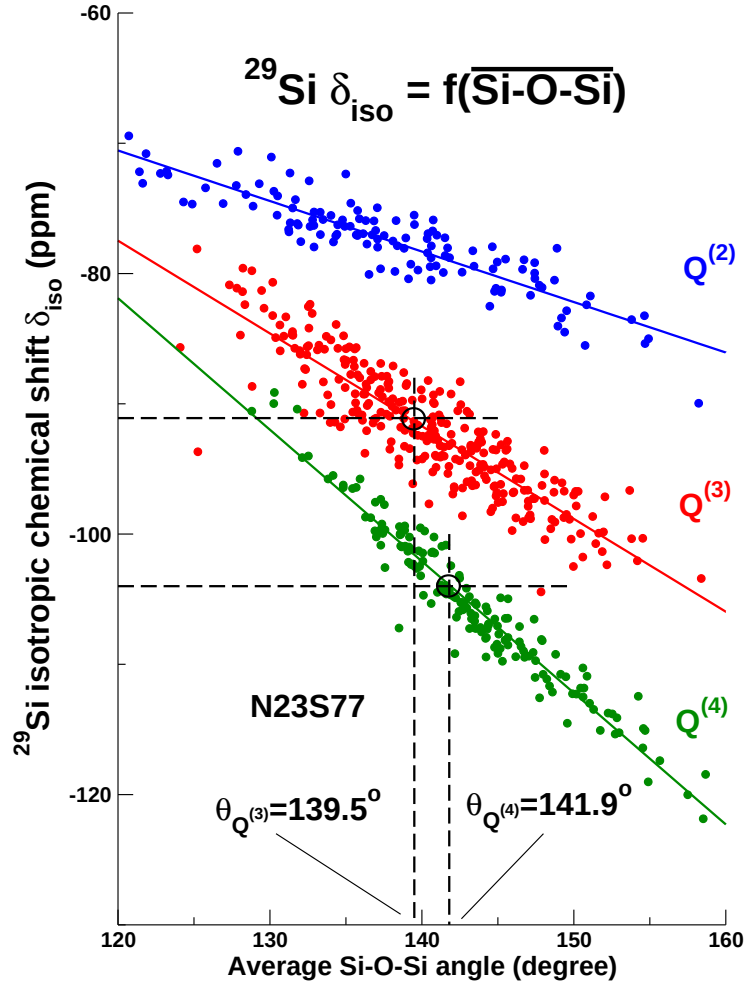

The NMR response of $Q^{(n)}$ species to disorder (bond angle distribution) is different.

Reconstructing the Bond Angle Distribution (BAD)

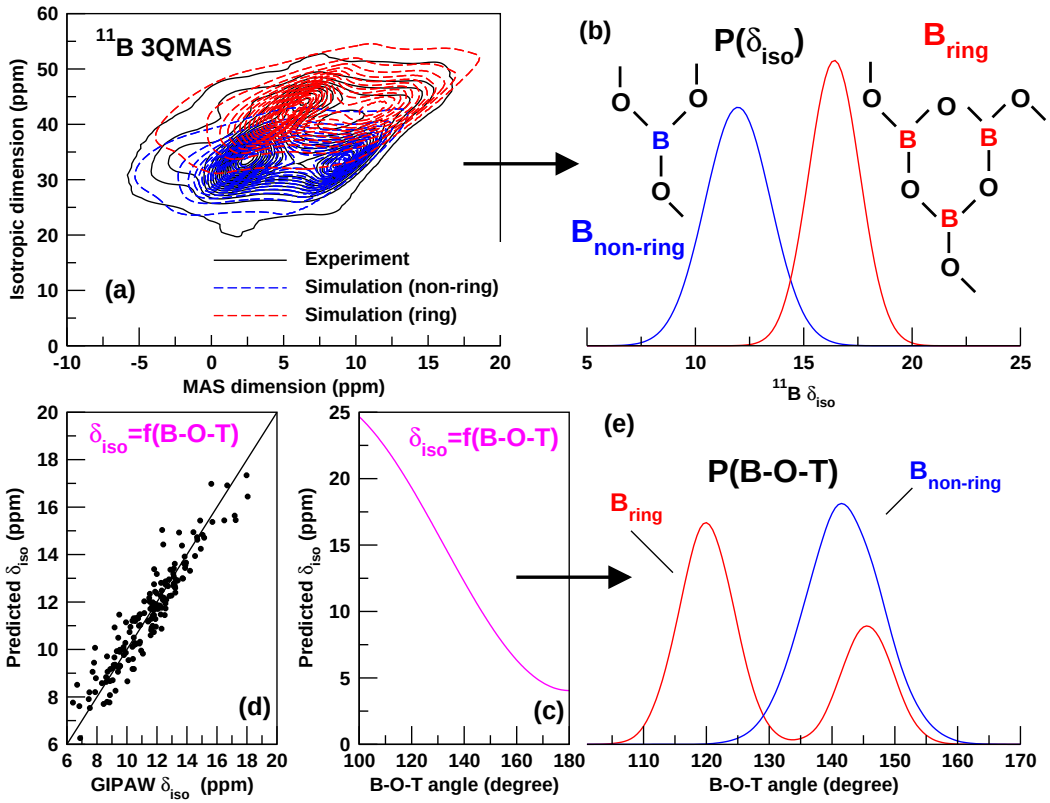

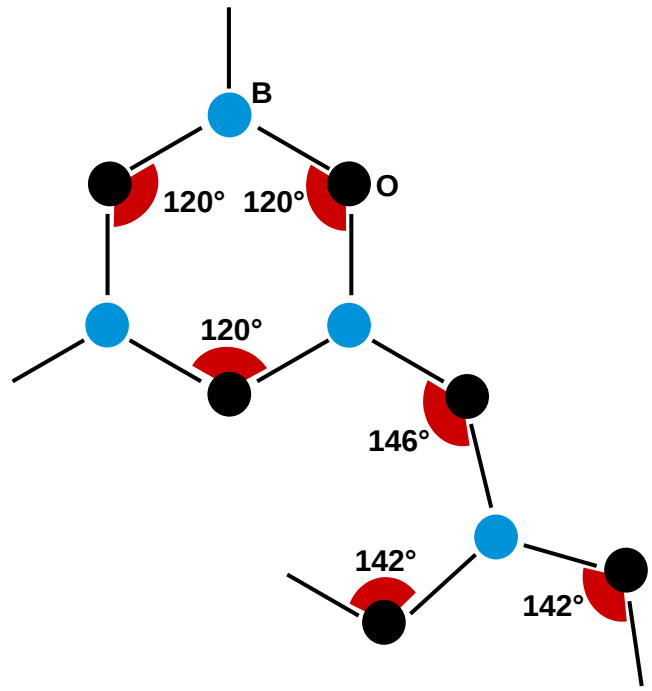

Magn. Reson. Chem. **48** 2010

- Vitreous SiO_2-B_2O_3 system
- ^{11}B NMR parameter distribution of BO_3 units
- ^{11}B NMR (δ_{iso}) vs B-O-(B,Si) bond angles

Through-Space correlation

Heteronuclear correlation

$$\frac{\hbar^2}{2} \sum_i \sum_{j \neq i} \gamma_i \gamma_j \vec{I}_i \left(\mathbf{D}_{ij} + \mathbf{J}_{ij} \right) \vec{I}_j$$

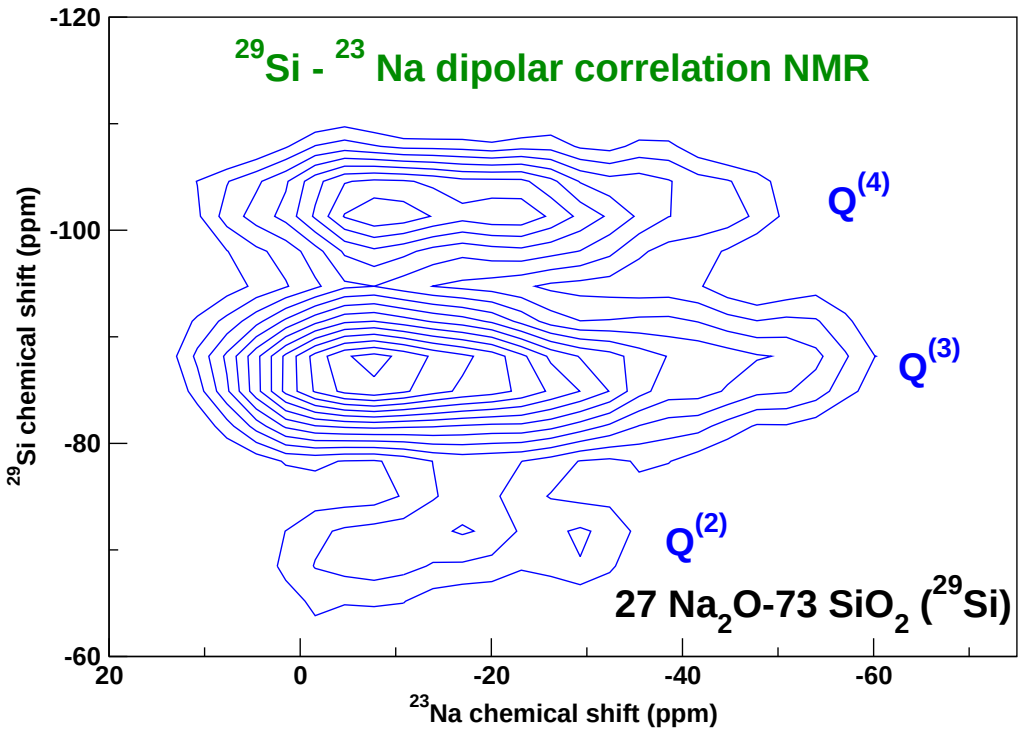

NMR of neighboring nuclear spins (Si-O$^-$ Na$^+$)

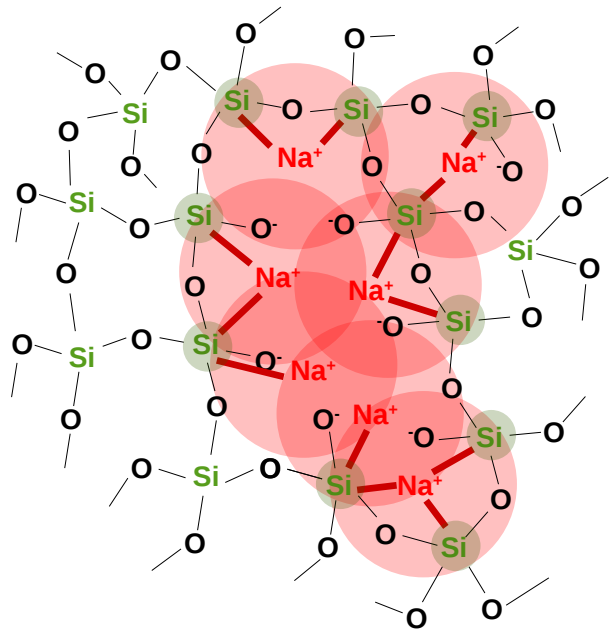

Through-Space correlation

Heteronuclear correlation

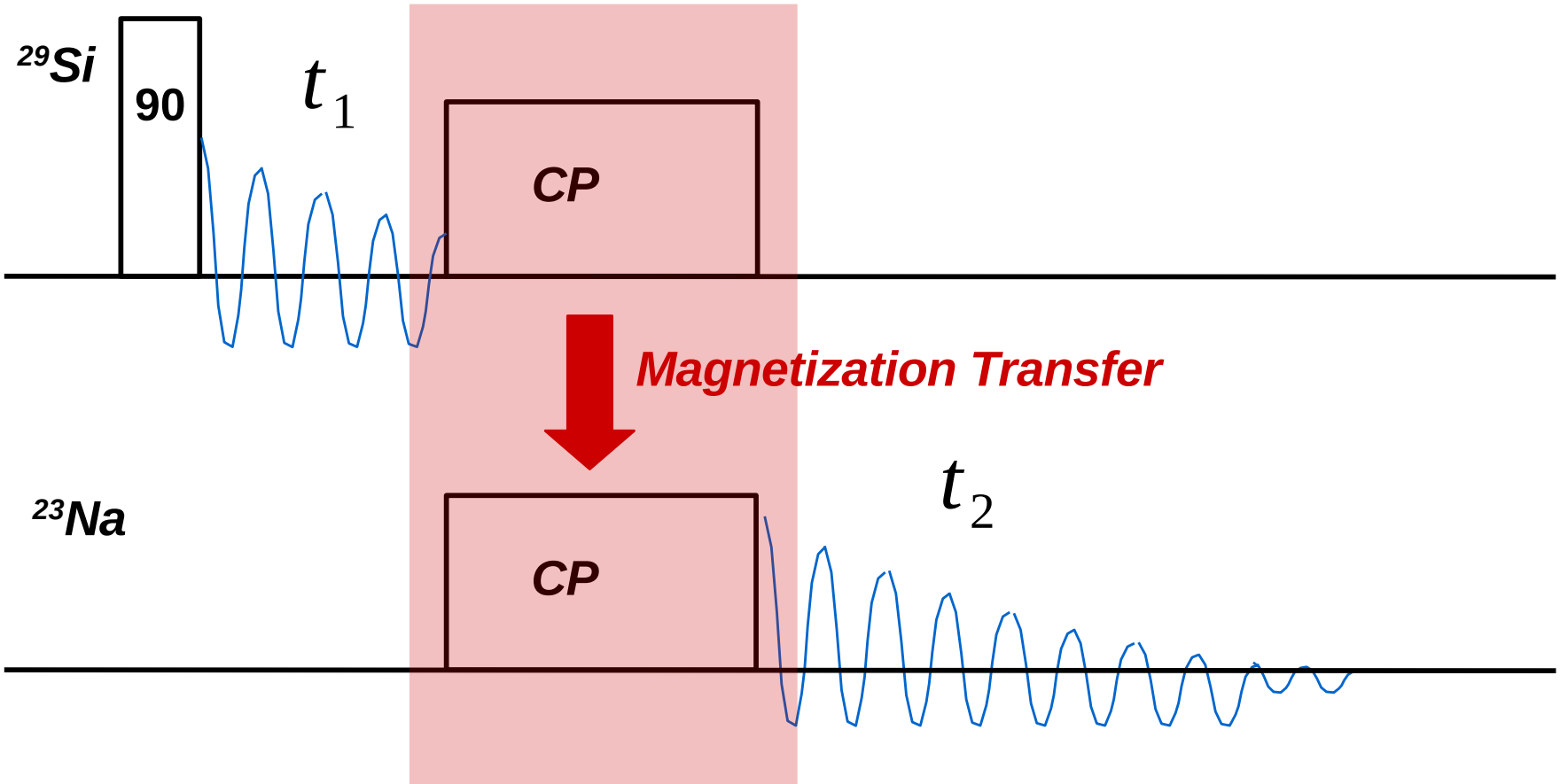

Through-bond correlation

$$\frac{\hbar^2}{2} \sum_i \sum_{j \neq i} \gamma_i \gamma_j \vec{I}_i \left(\mathbf{D}_{ij} + \mathbf{J}_{ij} \right) \vec{I}_j$$

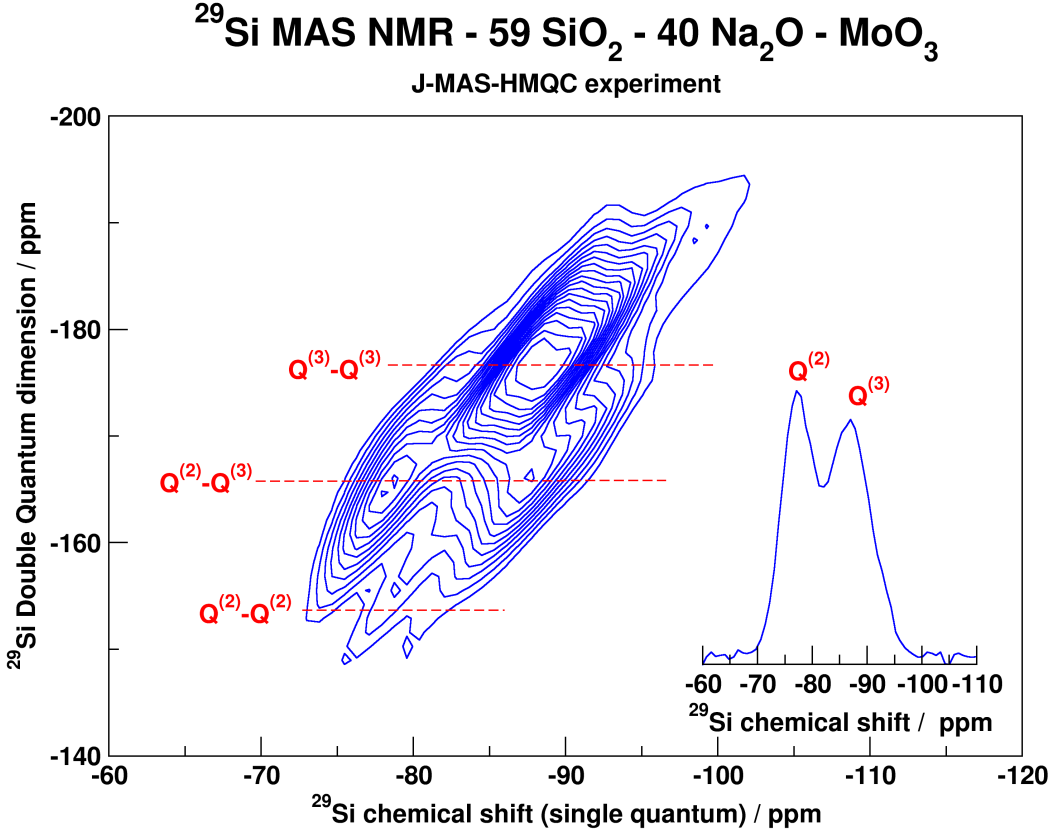

NMR of bonded nuclear spins (Si-O-Si)

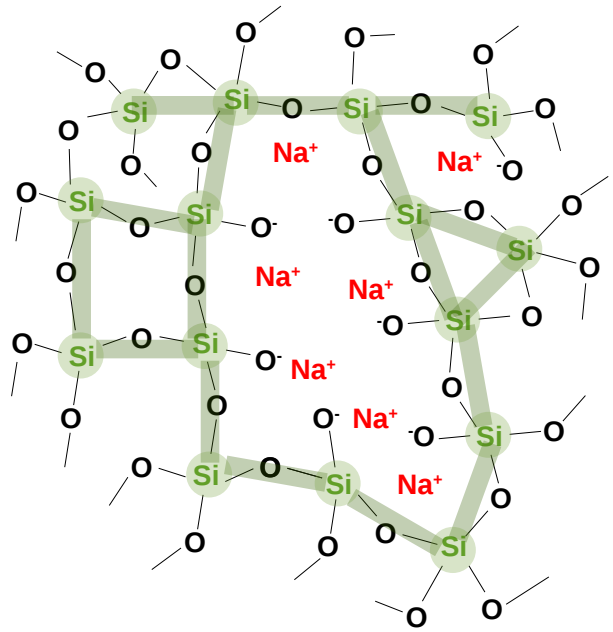

Through-bond correlation

Homonuclear correlation

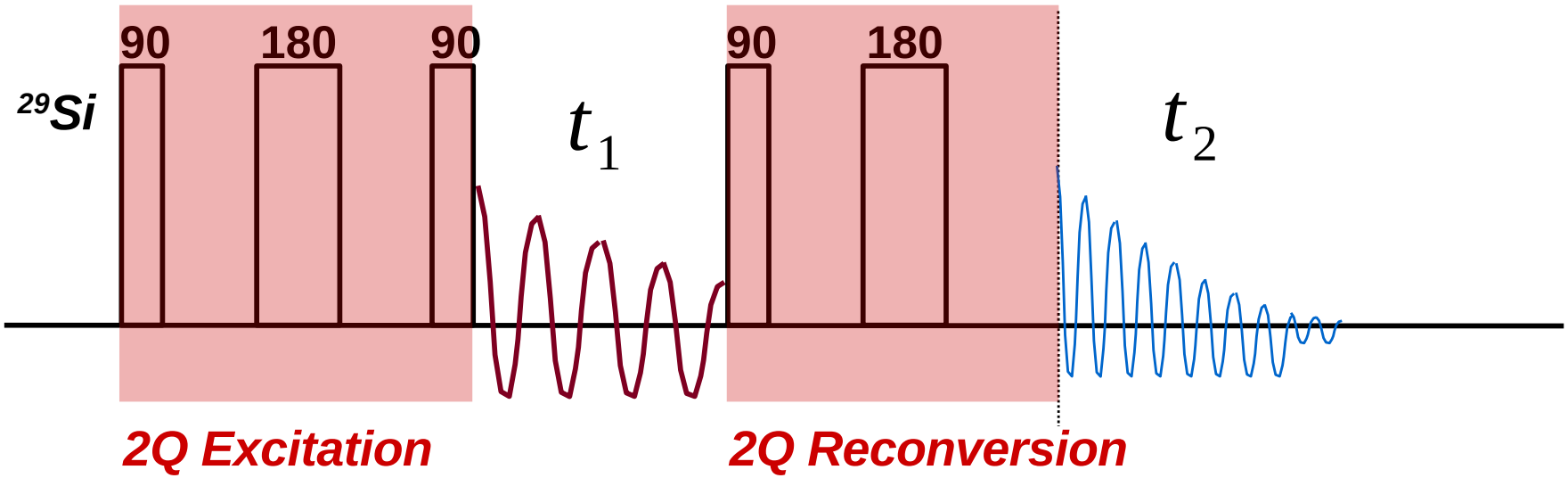

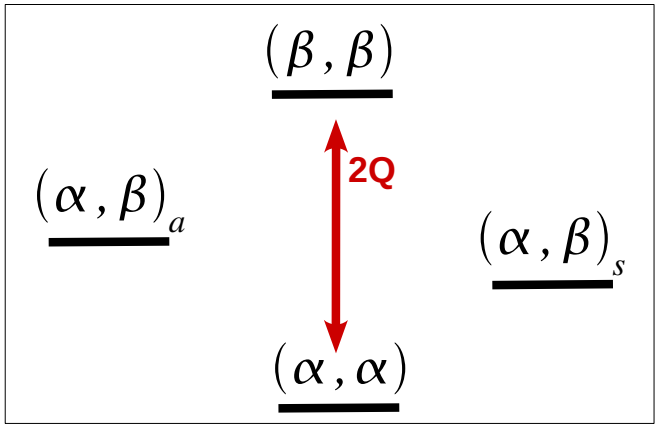

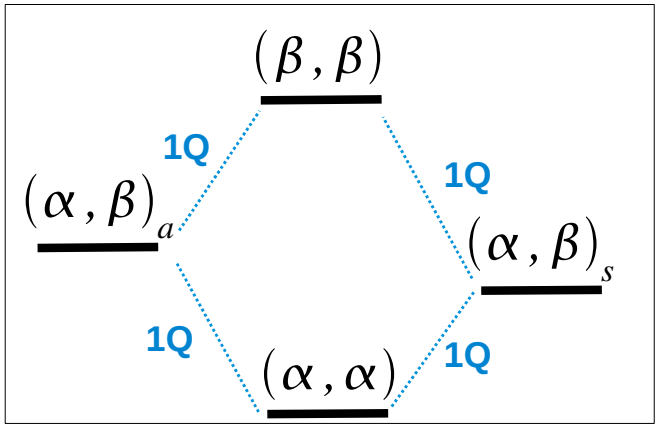

The MD GIPAW Methodology

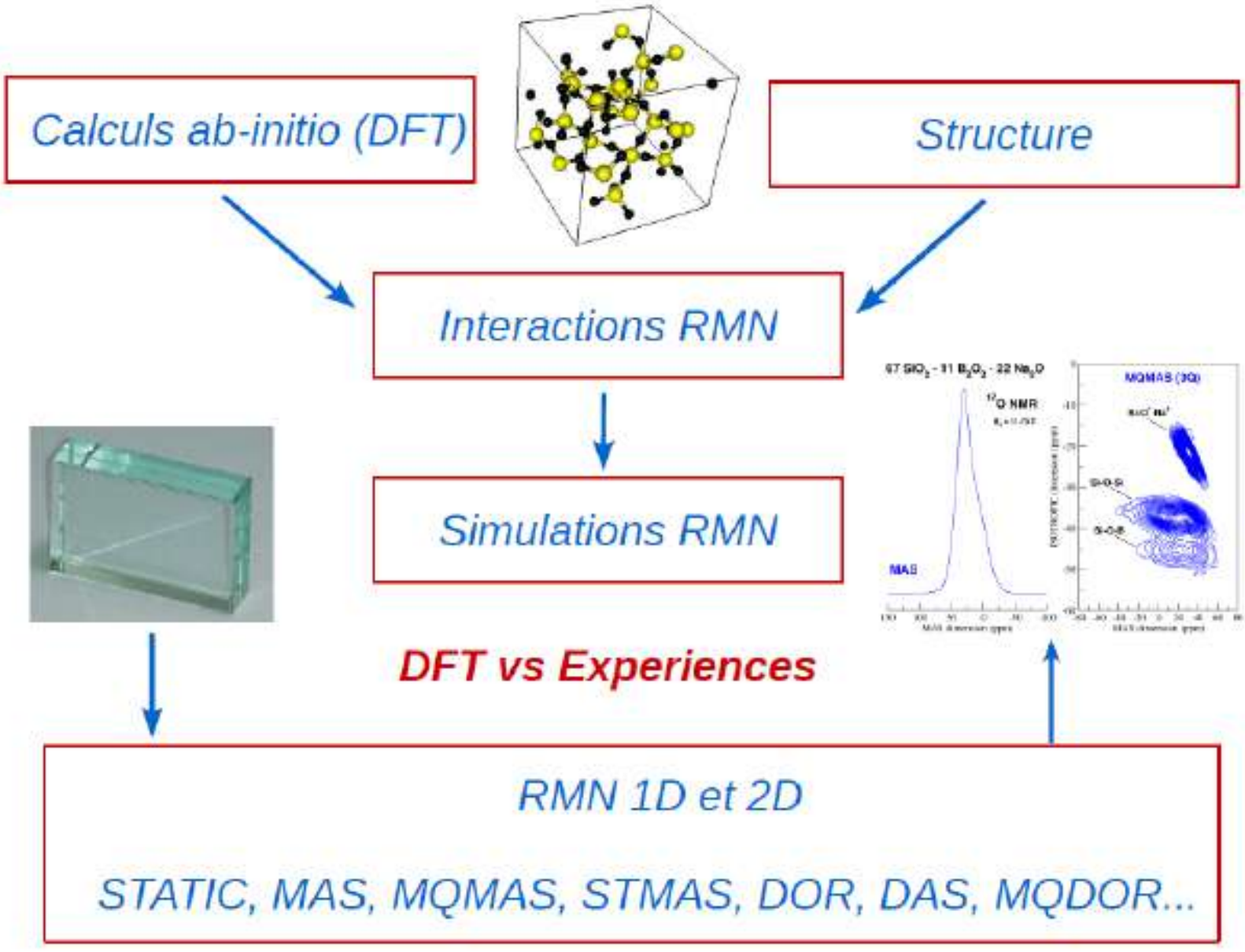

Supp: Perspective: MAS NMR at High Temperature

(F. Aussenac, Bruker; S. Schuller, CEA/DEN)

$60.4SiO_2 - 15.3B_2O_3 - 19Na_2O - 5.2CaO$ $57SiO_2 - 38Na_2O - 5MoO_3$

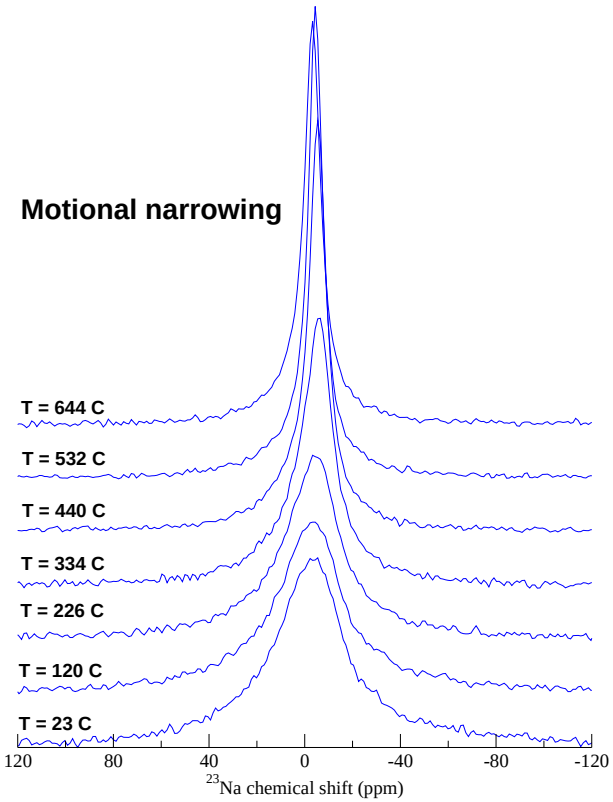

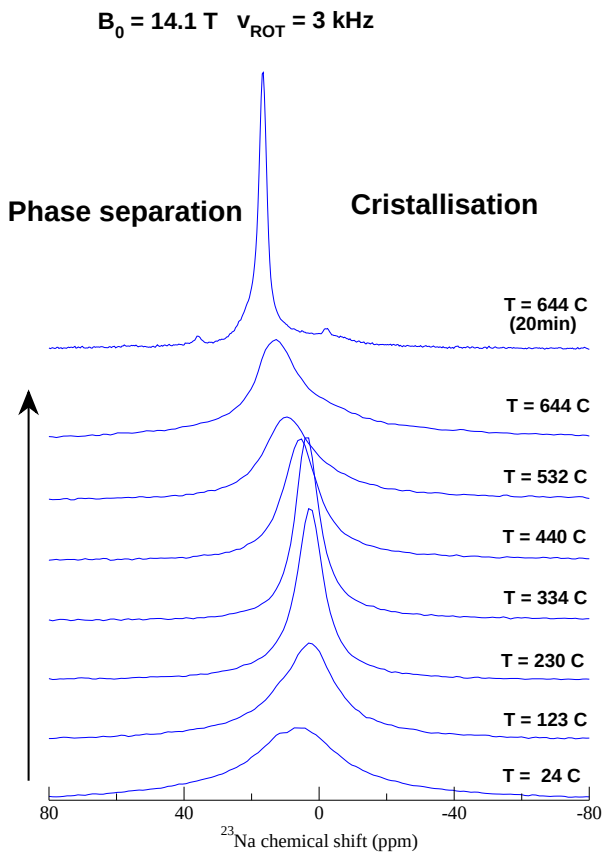

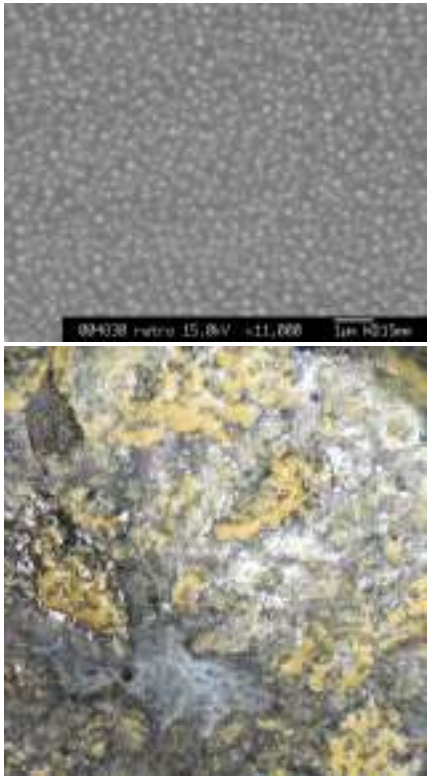

- New insights in cristallisation and glass demixion
- Introducing Dynamical effects in MD-GIPAW simulations

Solid State NMR of disordered materials at HT

(static) NMR HT

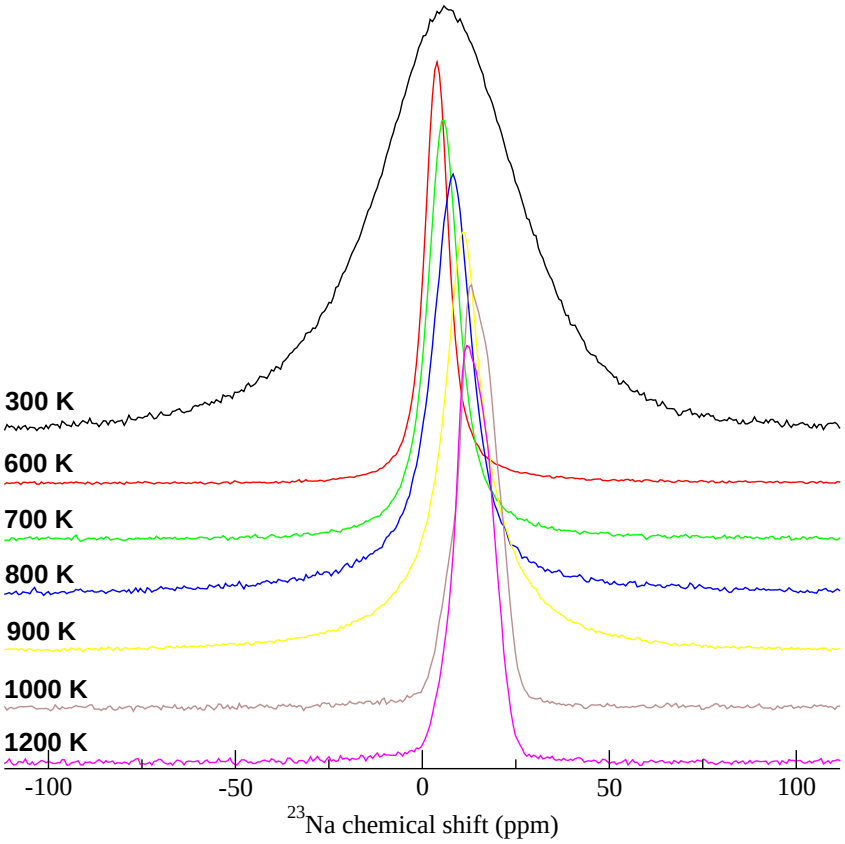

Data: 60 SiO_2 - 40 Na_2O Glass,

Longitudinal Relaxation T_1 (^{23}Na)

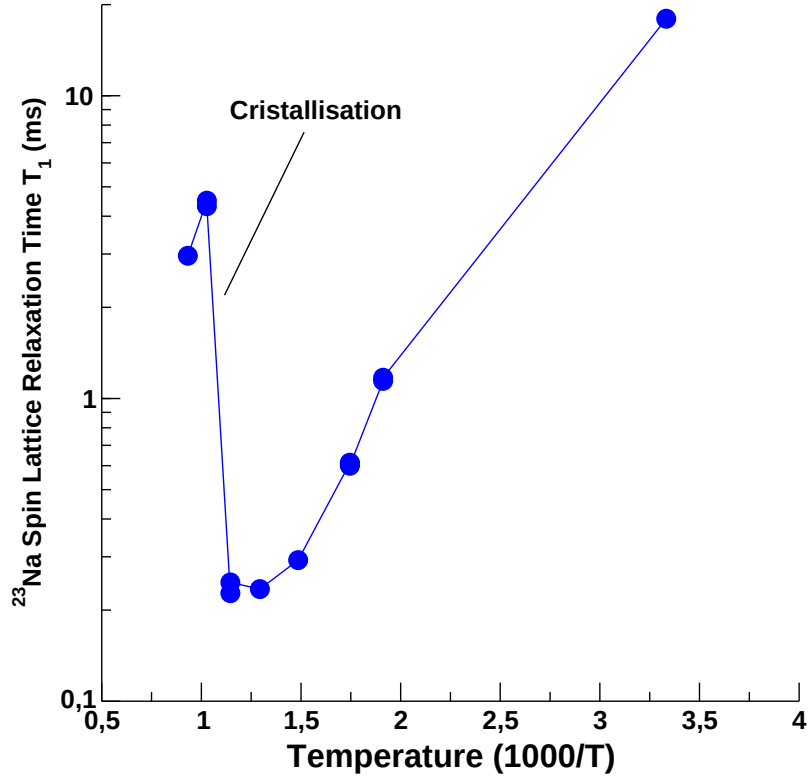

Coll. P. Florian, CEMHTI CNRS 750 MHz; S. Schuller, CEA/DEN.

MAS NMR at HT

High-temperature *in situ* ^{11}B NMR study of network dynamics in boron-containing glass-forming liquids

Jingshi Wu [a,*], Marcel Potuzak [b], Jonathan F. Stebbins [a]

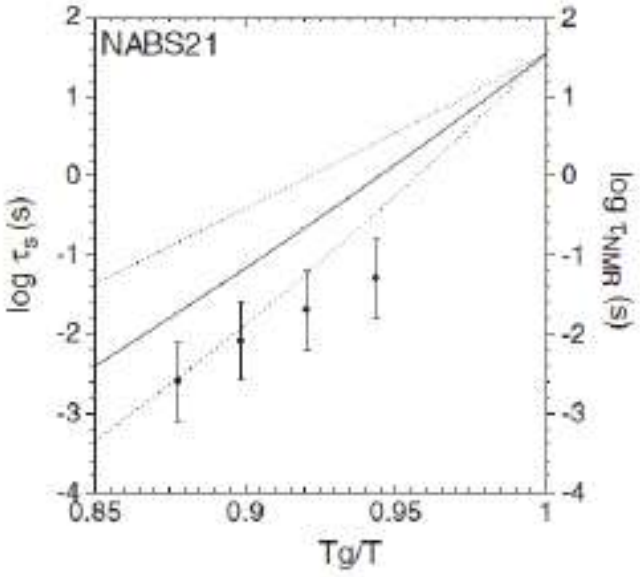

$$BO_4 = BO_3 + NBO$$

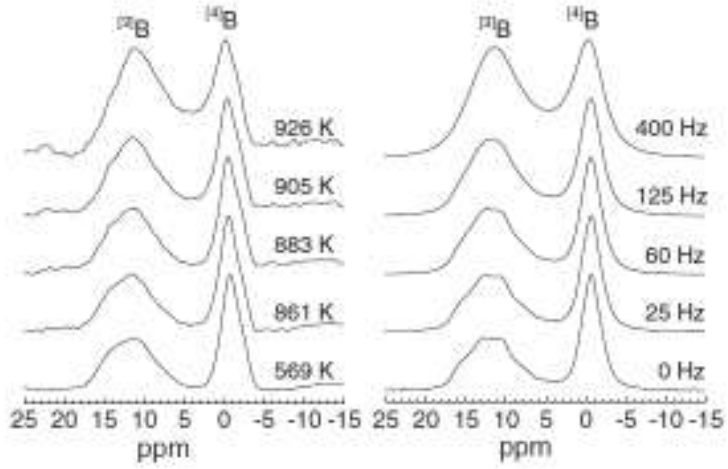

Fig. 3. High-temperature *in situ* ^{11}B MAS NMR spectra for a sodium aluminoborosilicate glass (NABS21), acquired at 14.1 T with a spinning speed of 5 kHz. Simulations using a multi-site exchange model are shown on the right, along with the mean exchange frequency $1/\tau_{NMR}$.

Journal of Non-Crystalline Solids 357 (2011) 3944–3951

Applications

Cite this: *Phys. Chem. Chem. Phys.*, 2011, **13**, 4540–4551

www.rsc.org/pccp

PAPER

Phase evolution in lithium disilicate glass–ceramics based on non-stoichiometric compositions of a multi-component system: structural studies by ^{29}Si single and double resonance solid state NMR

Christine Bischoff,†[a] Hellmut Eckert,*[a] Elke Apel,[b] Volker M. Rheinberger[b] and Wolfram Höland*[b]

System	SiO_2	Li_2O	Al_2O_3	K_2O	P_2O_5	ZrO_2
MKA	66.9	28.0	1.9	1.9	1.3	0.0
MKBp	66.0	27.6	1.9	1.9	1.3	1.3

Applications

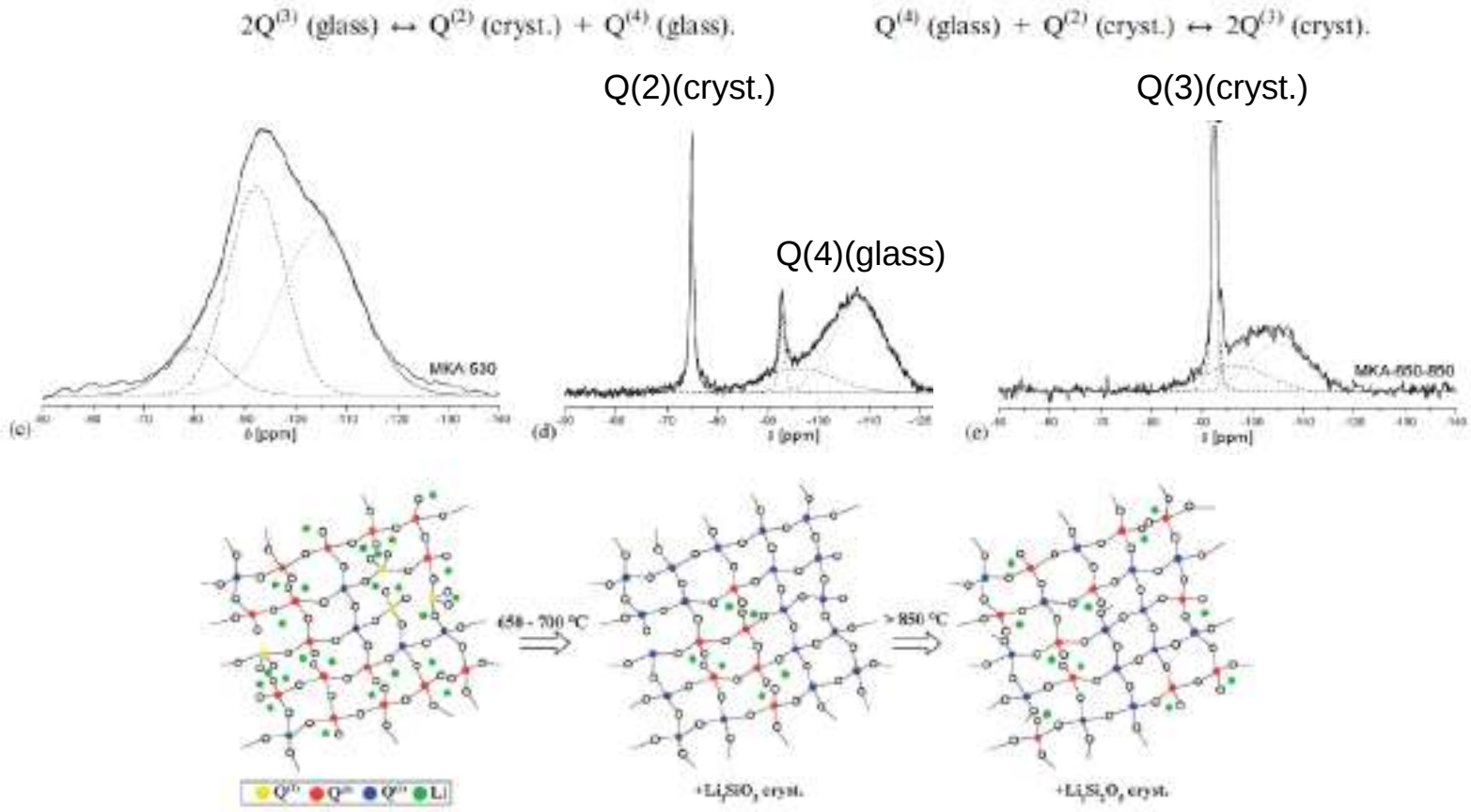

Fig. 11 Structural changes occurring in the remaining glassy phase during the two-stage crystallization of lithium disilicate glass. Left: starting glass; middle: remaining glass phase after Li_2SiO_3 crystallization near 650–700 °C; right: remaining glass phase after $Li_2Si_2O_5$ crystallization above 850 °C.

Applications

14618 *J. Phys. Chem. C* **2010**, *114*, 14618–14626

Glass-to-Vitroceramic Transition in the Yttrium Aluminoborate System: Structural Studies by Solid-State NMR

Heinz Deters,[†,‡] Andrea S. S. de Camargo,[†,§] Cristiane N. Santos,[§] and Hellmut Eckert*[,†]

TABLE 1: Compositions of the Undoped and the Paramagnetically Doped Yttrium Aluminoborate Vitroceramics

sample	RE_2O_3/ mol %	Y_2O_3/ mol %	Al_2O_3/ mol %	B_2O_3/ mol %
VC-Y10		10	30	60
VC-Y15		15	25	60
VC-Y20		20	20	60
VC-Y25		25	15	60

Applications

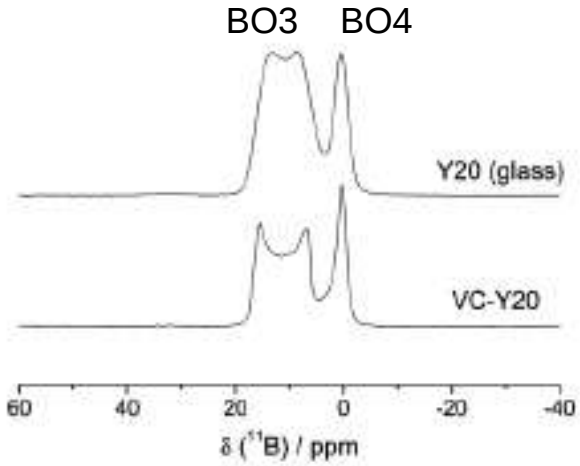

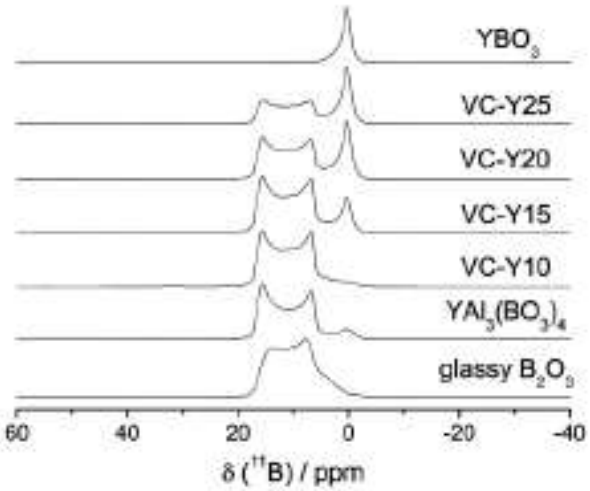

Figure 3. ^{11}B MAS NMR spectra of yttrium aluminoborate vitroceramics of crystalline YBO_3, $YAl_3(BO_3)_4$, and of glassy B_2O_3.

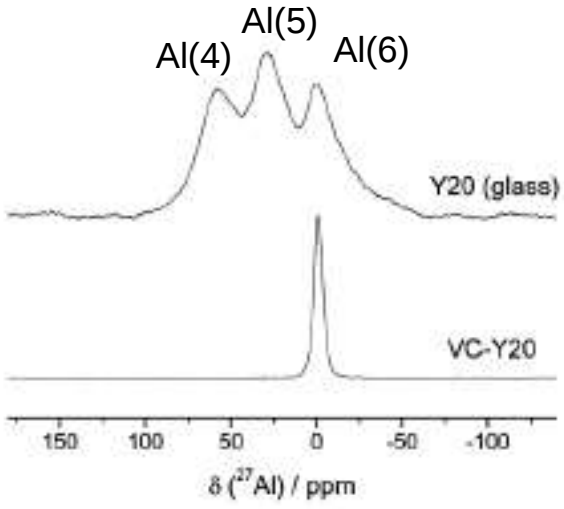

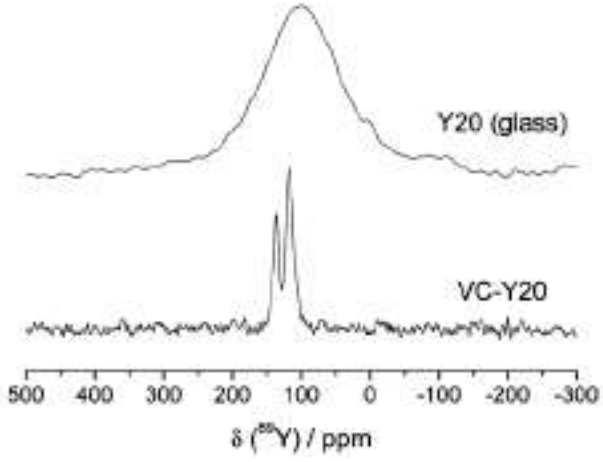

Applications

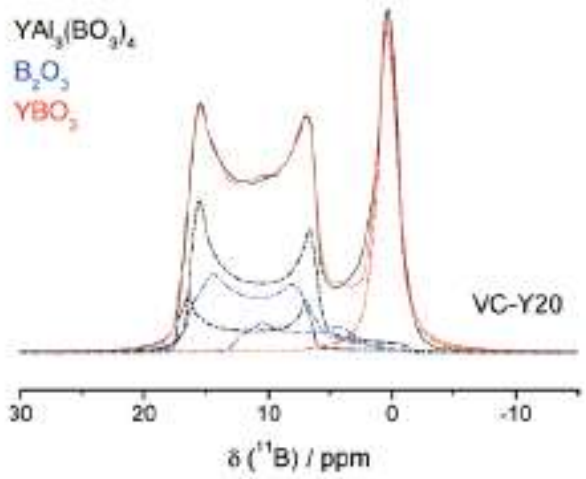

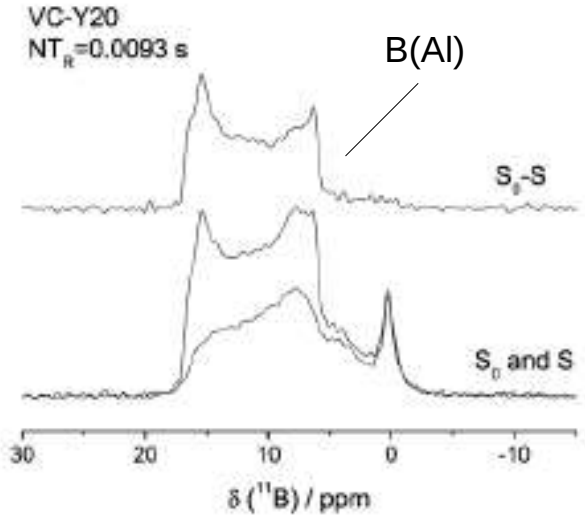

$$(B_2O_3)_{0.6}(Al_2O_3)_{0.4-y}(Y_2O_3)_y \rightarrow \{(0.8/3) - (2y/3)\}YAl_3(BO_3)_4 + \{(8y/3) - 0.8/3\}YBO_3 + 0.2B_2O_3 \quad (2)$$

Applications

Critical Reviews in Solid State and Materials Sciences, 36:229–241, 2011

ISSN: 1040-8436 print / 1547-6561 online
DOI: 10.1080/10408436.2011.593643

A Comparative Overview of Glass-Ceramic Characterization by MAS-NMR and XRD

Arvind Ananthanarayanan,[1,2] Gregory Tricot,[2] Govind Prasad Kothiyal,[1] and Lionel Montagne[2,*]

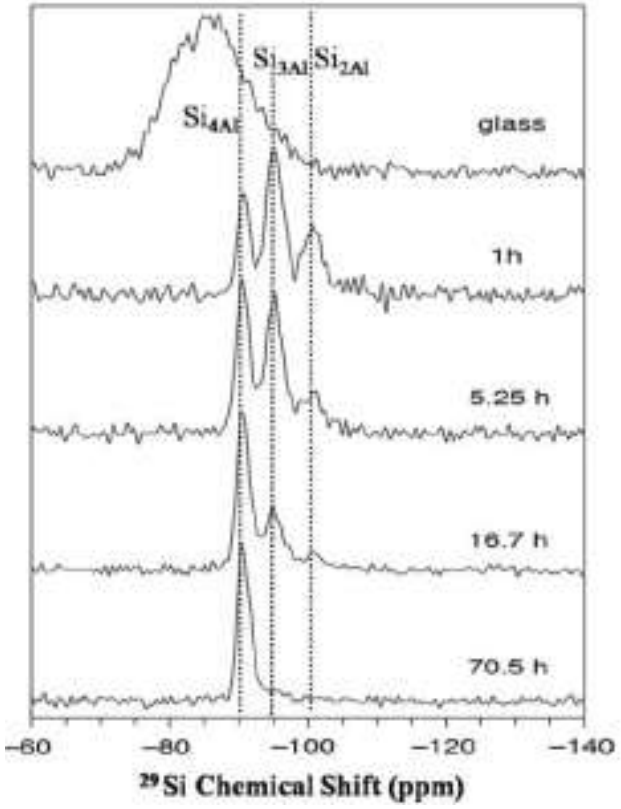

FIG. 7. ^{29}Si spectrum of a eucryptite glass crystallized at 900°C for different durations.[50] Considerable Si-Al disorder is evident in the early stages of crystallization. This leads to the resonances arising between -90 and -105 ppm corresponding to Si coordinated to different numbers of Al atoms.

50. B. L. Phillips, X. U. Hongwu, P. J. Heaney, and A. Navrotsky, ^{29}Si and ^{27}AlMAS-NMR spectroscopy of β-eucryptite ($LiAlSiO_4$): The enthalpy of Si,Al ordering *Am. Mineral.*, **85**, 181 (2000).

NMR / Bond Angle

IOP Publishing
Journal of Physics: Condensed Matter
J. Phys.: Condens. Matter 23 (2011) 284115 (17pp)
doi:10.1088/0953-8984/23/28/284115

Roles of bond orientational ordering in glass transition and crystallization

Hajime Tanaka

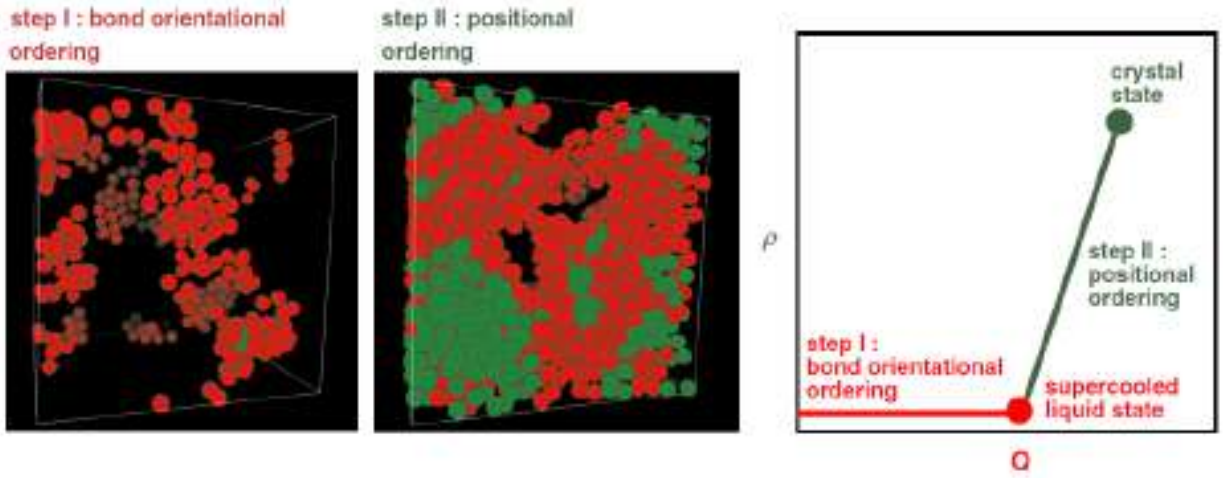

Aknowledgements

Glass

- O. Villain, A. Soleilhavoup (Post-doc), CEA/DSM/IRAMIS, France
- F. Angeli, P. Jollivet, S. Schuller, CEA/DEN/DTCD, France
- S. Peuget, O. Bouty, J.M. Delaye, CEA/DEN/DTCD, France
- D. Caurant, H. Trégouet, ENS Chimie Paris-Tech, France.

MD simulations / cp2k / Quantum Espresso

- M. Salanne, G. Ferlat, Université Paris 6, France
- S. Ispas, Laboratoire Charles Coulomb, Univ. Montpellier 2, France
- A. Seitsonen (Zürich)